Brain Pathology ISSN 1015-6305

RESEARCH ARTICLE

Reduction in the neuronal surface of post and presynaptic $GABA_B$ receptors in the hippocampus in a mouse model of Alzheimer's disease

Alejandro Martín-Belmonte[1]; Carolina Aguado[1]; Rocío Alfaro-Ruíz[1]; Ana Esther Moreno-Martínez[1]; Luis de la Ossa[2]; José Martínez-Hernández[1,*,†]; Alain Buisson[3]; Simon Früh[4]; Bernhard Bettler[4]; Ryuichi Shigemoto[5]; Yugo Fukazawa[6,7,8]; Rafael Luján[1,*]

[1] Synaptic Structure Laboratory, Instituto de Investigación en Discapacidades Neurológicas (IDINE), Departamento de Ciencias Médicas, Facultad de Medicina, Universidad Castilla-La Mancha, Campus Biosanitario, C/ Almansa 14, 02008, Albacete, Spain.
[2] Departamento de Sistemas Informáticos, Escuela Superior de Ingeniería Informática, Universidad de Castilla-La Mancha, 02071, Albacete, Spain.
[3] Grenoble Institut des Neurosciences, Université Grenoble Alpes, BP 170, Grenoble, France.
[4] Department of Biomedicine, Institute of Physiology, University of Basel, Basel, Switzerland.
[5] Institute of Science and Technology (IST Austria), Am Campus 1, A-3400, Klosterneuburg, Austria.
[6] Division of Brain Structure and Function, Faculty of Medical Science, University of Fukui, Fukui, Japan.
[7] Life Science Innovation Center, University of Fukui, Fukui, Japan.
[8] Research Center for Child Mental Development, Faculty of Medical Science, University of Fukui, Fukui, Japan.

Keywords
Alzheimer's disease, electron microscopy, freeze-fracture, $GABA_B$ receptors, hippocampus, immunohistochemistry, ion channels.

Corresponding author
Rafael Luján, Synaptic Structure Laboratory, Instituto de Investigación en Discapacidades Neurológicas (IDINE), Departamento de Ciencias Médicas, Facultad de Medicina, Universidad Castilla-La Mancha, Campus Biosanitario, C/ Almansa 14, 02008 Albacete, Spain. (E-mail: *Rafael.Lujan@uclm.es*)

*University of the Basque Country (UPV/EHU), 48940, Leioa, Spain.
†Ikerbasque, Basque Foundation for Science, 48013, Bilbao, Spain.

Received 2 July 2019
Accepted 4 November 2019
Published Online Article
Accepted 15 November 2019

doi:10.1111/bpa.12802

Abstract

The hippocampus plays key roles in learning and memory and is a main target of Alzheimer's disease (AD), which causes progressive memory impairments. Despite numerous investigations about the processes required for the normal hippocampal functions, the neurotransmitter receptors involved in the synaptic deficits by which AD disables the hippocampus are not yet characterized. By combining histoblots, western blots, immunohistochemistry and high-resolution immunoelectron microscopic methods for $GABA_B$ receptors, this study provides a quantitative description of the expression and the subcellular localization of $GABA_{B1}$ in the hippocampus in a mouse model of AD at 1, 6 and 12 months of age. Western blots and histoblots showed that the total amount of protein and the laminar expression pattern of $GABA_{B1}$ were similar in APP/PS1 mice and in age-matched wild-type mice. In contrast, immunoelectron microscopic techniques showed that the subcellular localization of $GABA_{B1}$ subunit did not change significantly in APP/PS1 mice at 1 month of age, was significantly reduced in the *stratum lacunosum-moleculare* of CA1 pyramidal cells at 6 months of age and significantly reduced at the membrane surface of CA1 pyramidal cells at 12 months of age. This reduction of plasma membrane $GABA_{B1}$ was paralleled by a significant increase of the subunit at the intracellular sites. We further observed a decrease of membrane-targeted $GABA_B$ receptors in axon terminals contacting CA1 pyramidal cells. Our data demonstrate compartment- and age-dependent reduction of plasma membrane-targeted $GABA_B$ receptors in the CA1 region of the hippocampus, suggesting that this decrease might be enough to alter the $GABA_B$-mediated synaptic transmission taking place in AD.

INTRODUCTION

Alzheimer's disease (AD) is the most prevalent neurodegenerative disease in the elderly population. Alzheimer's disease progression has been associated with a gradual damage in function and structure of the hippocampus, a vulnerable brain region involved in the memory formation and in the cognition. In particular, the CA1 hippocampal region is one of the most affected brain areas in AD, suffering a variety of neuronal alterations, including dendritic changes in pyramidal cells and pronounced loss of neurons (55, 56). The three major neuropathology hallmarks of AD are extracellular amyloid plaques containing amyloid β (Aβ) peptides derived from amyloid precursor protein (APP), neurofibrillary tangles of aggregated hyperphosphorylated tau in neurons and synapse loss (5). The progressive increase in synapse

loss correlates with cognitive decline and is proposed to underlie learning and memory deficits in AD (21).

Amyloid β (Aβ) has been implicated in the pathogenesis of AD by creating a microenvironment that damages the dendritic spines, which represent the major postsynaptic elements of excitatory synapses in the cerebral cortex (16), and are fundamental to memory formation, learning and cognition (30). Growing evidence supports that structural plasticity impairments on excitatory synapses are linked to a gross disruption of the glutamatergic system (36, 41, 55, 58, 59). Thus, N-methyl-D-aspartate (NMDA) receptors activation and removal of AMPA receptors have been implicated in AD-related synaptic dysfunctions (20, 59). The neurotransmitter γ-aminobutyric acid (GABA) acts through $GABA_A$ and $GABA_B$ receptors to inhibit neurons (3, 13). While alterations in the expression of $GABA_A$ receptor subunits in the AD hippocampus differ (28) alterations in $GABA_B$ receptor expression are less well understood and only recently it has been shown a direct molecular and functional link between APP and $GABA_B$ receptors (9, 45, 47).

$GABA_B$ receptors have modulatory actions on neuronal excitability and neurotransmitter release, and are involved in a number of physiological and pathophysiological processes (3), including AD. Two subunits, $GABA_{B1}$ and $GABA_{B2}$, are required to form functional receptors (26, 37). Autoradiographic, *in situ* hybridisation and immunohistochemical studies showed that the hippocampus expresses a high-density of $GABA_B$ receptors (4, 6, 7, 12, 25, 32). Immunoelectron microscopic studies demonstrated an association of $GABA_B$ receptors with postsynaptic and presynaptic sites at excitatory synapses in the hippocampus, with a particularly high abundance in the dendritic spines of pyramidal cells (8, 27, 32, 53). Since dendritic spines and excitatory synapses are lost in AD it is expected that both the distribution and functions of $GABA_B$ receptors are affected. However, it remains unclear how these receptors reorganize at the surface of hippocampal neurons in AD brains. For this purpose, our work adopted transgenic mice overexpressing mutant familial AD genes [amyloid-β protein precursor (AβPP), presenilin-1 (PS1)-dE9], considered one of the most relevant animal models of AD. These animals show Aβ deposition by 4 months with a progressive increase in senile plaque number up to 12 months and cognitive impairments (14, 15).

To identify possible alterations in the expression and subcellular localization of $GABA_B$ receptors in the APP/PS1 mice we used western blots, histoblots and high-resolution immunohistochemical techniques in combination with quantitative approaches at different ages. Here we provide evidence for a significant reduction in the plasma membrane expression of $GABA_B$ receptors in CA1 pyramidal cells in the APP/PS1 AD mouse model.

MATERIAL AND METHODS

Animals

The mouse line used for this study (APP/PS1; hemizygote animals) expressed Mo/Hu APP695swe construct in conjunction with the exon 9-deleted variant of human presenilin 1 (PS1-dE9) (46). Control mice were age-matched littermates without the transgene (wild type). Mice of all genotypes were aged to 1, 6 and 12 months before use in a battery of biochemical and morphological experiments. For each age and genotype, four mice were used for western blot, four mice were used for histoblot techniques, four mice were used for SDS-FRL techniques and three mice were used for pre-embedding immunoelectron microscopic analyses. All mice were obtained from the Animal House Facility of the University of Castilla-La Mancha (Albacete, Spain). Animals were housed in cages of 2 or more mice, maintained on a 12 hour light/12 hour dark cycle at 24°C and received food and water *ad libitum*. Care and handling of animals prior to and during experimental procedures were in accordance with Spanish (RD 1201/2015) and European Union regulations (86/609/EC), and the protocols were approved by the local Animal Care and Use Committee.

For western blots, the animals were deeply anesthetized by intraperitoneal injection of ketamine/xylazine 1:1 (0.1 mL/kg b.w.), the hippocampus was extracted, frozen rapidly in liquid nitrogen and stored at −80°C. For histoblotting, the animals were deeply anesthetized by intraperitoneal injection of ketamine/xylazine 1:1 (0.1 mL/kg b.w.), the brains were quickly frozen in liquid nitrogen and stored at −80°C. For immunohistochemistry at the light and electron microscopic levels, animals were deeply anesthetized by intraperitoneal injection of ketamine-xylazine 1:1 (0.1 mL/kg) and transcardially perfused with ice-cold fixative containing: (i) 2% paraformaldehyde in 0.1 M phosphate buffer (PB, pH 7.4) for 12 min (for SDS-FRL technique), or (ii) 4% paraformaldehyde, 0.05% glutaraldehyde and 15% (v/v) saturated picric acid made up in 0.1 M phosphate buffer (PB), pH 7.4 (for light microscopy and pre-embedding immunogold techniques). After perfusion, brains were removed and immersed in the same fixative for 2 h or overnight at 4°C. Tissue blocks were washed thoroughly in 0.1 M PB. Coronal sections (60 μm thickness) were cut on a Vibratome (Leica V1000).

Antibodies and chemicals

An affinity-purified polyclonal antibody against $GABA_{B1}$ (B17, aa. 901-960 of rat $GABA_{B1}$) was raised in rabbit, and used for immunohistochemical techniques at the light and electron microscopic levels. The characteristics and specificity of the anti-$GABA_{B1}$ antibody have been described elsewhere (26, 35, 53). For western blots and histoblots, a mouse monoclonal anti-$GABA_{B1}$ (sc-166408; D-2, aa 929-958 of rat C-terminus of $GABA_{B1}$) antibody was used (Santa Cruz, CA, USA), and we provided additional information on its specificity. A monoclonal anti-α-Tubulin (DM1A; ref CP06) was obtained from Millipore (Millipore Corporation, Burlington, MA, USA). An affinity-purified polyclonal antibody against β-amyloid (ref #2454, detecting human Aβ-40 and Aβ-42 peptides) raised in rabbit was obtained from Cell Signalling Technology (Leiden, The Netherlands).

The secondary antibodies used were as follows: goat anti-mouse IgG-horseradish peroxidase (1:2000; Santa Cruz Biotechnology, Santa Cruz, CA, USA), goat anti-rabbit IgG-horseradish peroxidase (1:15 000; Pierce, Rockford,

USA), alkaline phosphatase AP-goat anti-mouse IgG (H + L) and AP-goat anti-rabbit IgG (H + L) (1:5000; Invitrogen, Paisley, UK), goat anti-rabbit IgG coupled to 1.4 nm gold (1:100; Nanoprobes Inc., Stony Brook, NY, USA) and anti-rabbit IgG conjugated to 10 nm gold particles (1:100; British Biocell International, Cardiff, UK).

Western blots

Hippocampi were homogenized in 50 mM Tris Base, pH 7.4 and Protease Inhibitor Cocktail (Thermo Scientific, Pierce, Rockford, USA) with a pestle motor (Sigma-Aldrich). The homogenized tissue was centrifuged 10 min at 1000 × *g* at 4°C and the supernatant was centrifuged 30 min at 12000 × *g* (Centrifuge 5415R, Eppendorf, Hamburg, Germany) at 4°C, the pellet containing the membrane extracts were resuspended in 50 mM Tris Base, pH 7.4 and Protease Inhibitor Cocktail (Thermo Scientific, Pierce, Rockford, USA). The protein content of each membrane extract was determined by BCA Protein Assay Kit (Thermo Scientific). Twenty-five micrograms of membrane protein were loaded in Sodium dodecyl sulfate polyacrylamide gel electrophoresis (SDS/PAGE) using 7.5% polyacrylamide with loading sample buffer (0,05 M Tris pH 6.8, 2% SDS, 10% glycerol, 0,05% β-mercaptoethanol and 0,001% bromophenol blue). The proteins were transferred to PVDF membranes using a semidry transfer system and immunoblotted with anti-$GABA_{B1}$ (1:500) and anti-α-Tubulin (1:1000). Protein bands were visualized after application of a mouse IgG kappa-binding protein coupled to horseradish peroxidase (1:1000) using the enhanced chemiluminescence (ECL) blotting detection kit (SuperSignal West Dura Extended Duration Substrate, Pierce, Rockford, USA). Blots were captured and quantified by densitometry using a LAS4000 MINI (Fujifilm, Japan). A series of primary and secondary antibody dilutions and incubation times were used to optimize the experimental conditions for the linear sensitivity range, confirming that our labeling was well below the saturation levels.

Histoblotting

The regional distribution of $GABA_{B1}$ was analysed in rodent brains, using an *in situ* blotting technique (histoblot) (1, 52). Briefly, horizontal cryostat sections (10 μm) from mouse brain were apposed to nitrocellulose membranes moistened with 48 mM Tris-base, 39 mM glycine, 2% (w/v) sodium dodecyl sulphate and 20% (v/v) methanol for 15 min at room temperature (~20°C). After blocking in 5% (w/v) nonfat dry milk in phosphate-buffered saline, nitrocellulose membranes were treated with DNAse I (5 U/mL), washed and incubated in 2% (w⁄v) sodium dodecyl sulphate and 100 mm β-mercaptoethanol in 100 mM Tris–HCl (pH 7.0) for 60 min at 45°C to remove adhering tissue residues. After extensive washing, the blots were reacted with affinity-purified anti-$GABA_{B1}$ antibodies (0.5 mg⁄mL) in blocking solution overnight at 4°C. The bound primary antibodies were detected with alkaline phosphatase-conjugated anti-rabbit IgG secondary antibodies (52). A series of primary and secondary antibody dilutions and incubation times were used to optimize the experimental conditions for the linear sensitivity range of the alkaline phosphatase reactions. To compare the expression levels of $GABA_{B1}$ between the two genotypes (wild type and APP/PS1) and ages (1, 6 and 12-months), all nitrocellulose membranes were processed in parallel, and the same incubation time for each reagent was used for the antibody.

To facilitate the identification of brain regions, structures and cell layers, adjacent cryostat sections were stained with cresyl violet for the two genotypes (wild type and APP/PS1) and ages (1, 6 and 12-months; not shown). Digital images were acquired by scanning the nitrocellulose membranes using a desktop scanner (HP Scanjet 8300). Image analysis and processing were performed using the Adobe Photoshop software (Adobe Systems, San Jose, CA, USA) as described previously (10). All of the images were processed with the same equipment in the same way to allow comparison of the intensity of grayscale images between experimental groups and in different brain regions. The pixel density (arbitrary units) of immunoreactivity was measured using open circular cursors with a diameter of 0.10 mm. The cursors were placed in different brain regions identified based on the adjacent cresyl violet-stained sections (10). We used background correction to eliminate the potential differences in optical densities across different sections in different experiments. The average of eight background determinations carried out near the brain protein-containing areas of the immunostained nitrocellulose membranes was subtracted from the average pixel densities measured within the brain regions. Following background corrections, the average pixel density for the whole region from one animal counted as one 'n'. Under these conditions, labeling performed on different days produced very consistent results. Data were analyzed and plotted using the software Analysis (GraphPad Prism, San Diego, USA).

Immunohistochemistry for light microscopy

Immunohistochemical reactions at the light microscopic level were carried out using the immunoperoxidase method as described earlier (34). Briefly, sections were incubated in 10% normal goat serum (NGS) diluted in 50 mM Tris buffer (pH 7.4) containing 0.9% NaCl (TBS), with 0.2% Triton X-100, for 1 h. Sections were incubated in anti-$GABA_{B1}$ (1–2 μg/mL diluted in TBS containing 1% NGS) or in anti-β amyloid (1–2 μg/mL diluted in TBS containing 1% NGS), followed by incubation in biotinylated goat anti-rabbit IgG (Vector Laboratories, Burlingame, CA) diluted 1:200 in TBS containing 1% NGS. Sections were then transferred into avidin–biotin–peroxidase complex (ABC kit, Vector Laboratories). Bound peroxidase enzyme activity was revealed using 3,3′-diaminobenzidine tetrahydrochloride (DAB; 0.05% in TB, pH 7.4) as the chromogen and 0.01% H_2O_2 as the substrate. Finally, sections were air-dried and

mounted prior to observation in a Leica photomicroscope (DM2000) equipped with differential interference contrast optics and a digital imaging camera.

Immunohistochemistry for electron microscopy

Immunohistochemical reactions at the electron microscopic level were carried out using the pre-embedding immunogold and the SDS-digested freeze-fracture replica labeling (SDS-FRL) methods as described earlier (33, 34, 50).

Pre-embedding immunogold method. Briefly, free-floating sections obtained from the two genotypes (WT and APP/PS1) and three ages (1, 6 and 12-months) were incubated in parallel in 10% (v/v) NGS diluted in TBS. Sections were then incubated in anti-$GABA_{B1}$ antibodies (3-5 μg/mL diluted in TBS containing 1% (v/v) NGS), followed by incubation in goat anti-rabbit IgG coupled to 1.4 nm gold (Nanoprobes Inc., Stony Brook, NY, USA), respectively. Sections were postfixed in 1% (v/v) glutaraldehyde and washed in double-distilled water, followed by silver enhancement of the gold particles with an HQ Silver kit (Nanoprobes Inc.). Sections were then treated with osmium tetraoxide (1% in 0.1 M phosphate buffer), block-stained with uranyl acetate, dehydrated in graded series of ethanol and flat-embedded on glass slides in Durcupan (Fluka) resin. Regions of interest were cut at 70–90 nm on an ultramicrotome (Reichert Ultracut E, Leica, Austria) and collected on single slot pioloform-coated copper grids. Staining was performed on drops of 1% aqueous uranyl acetate followed by Reynolds's lead citrate. Ultrastructural analyses were performed in a JEOL-1010 electron microscope.

SDS-FRL technique. Animals were anesthetized with sodium pentobarbital (50 mg/kg, i.p.) and perfused transcardially with 25 mM PBS for 1 min, followed by perfusion with 2% paraformaldehyde in 0.1 M phosphate buffer (PB) for 12 min. The hippocampi were dissected and cut into sagittal slices (130 μm) using a Microslicer (Dosaka, Kyoto, Japan) in 0.1 M PB. Next, we trimmed hippocampal slices containing the CA region and immersed them in graded glycerol of 10%–30% in 0.1 M PB at 4°C overnight. Slices were frozen using a high-pressure freezing machine (HPM010, BAL-TEC, Balzers). Slices were then fractured into two parts at -120°C and replicated by carbon deposition (5 nm thick), platinum (60° unidirectional from horizontal level, 2 nm) and carbon (15-20 nm) in a freeze-fracture replica machine (BAF060, BAL-TEC, Balzers). Replicas were transferred to 2.5% SDS and 20% sucrose in 15 mM Tris buffer (pH 8.3) for 18 h at 80°C with shaking to dissolve tissue debris. The replicas were washed three times in 50 mM Tris-buffered saline (TBS, pH 7.4), containing 0.05% bovine serum albumin (BSA) and then blocked with 5% BSA in the washing buffer for 1 h at room temperature. Next, the replicas were washed and reacted with a polyclonal rabbit antibody for $GABA_{B1}$ (5μg/mL) at 15°C overnight. Following three washes in 0.05% BSA in TBS and blocking in 5% BSA/TBS, replicas were incubated in secondary antibodies conjugated with 10 nm gold particles overnight at room temperature. When the primary antibody was omitted, no immunoreactivity was observed. After immunogold labeling, the replicas were immediately rinsed three times with 0.05% BSA in TBS, washed twice with distilled water and picked up onto grids coated with pioloform (Agar Scientific, Stansted, Essex, UK).

Quantification and analysis of SDS-FRL data

The labeled replicas were examined using a transmission electron microscope (JEOL-1010) and photographed at magnifications of 60,000, 80,000 and 100,000. All antibodies used in this study were visualized by immunoparticles on the protoplasmic face (P-face), consistent with the intracellular location of their epitopes. Nonspecific background labeling was measured on E-face surfaces in wild-type mice. Digitised images were then modified for brightness and contrast using Adobe PhotoShop CS5 (Mountain View, CA, USA) to optimize them for quantitative analysis. The quantitative analyses were done using the software GPDQ (*Gold Particle Detection and Quantification*) developed recently to perform automated and semiautomated detection of gold particles present in a given compartment of neurons (33).

Density gradient of $GABA_{B1}$ along the membrane surface. The procedure was similar to that used previously (33). Briefly, immunogold labeling for $GABA_{B1}$ was achieved from replicas containing all layers of the CA1 region, so that the laminar distribution could be compared under identical conditions for each animal and experimental group. Quantitative analysis of immunogold labeling for $GABA_{B1}$ was performed on ten different dendritic compartments of pyramidal cells in all dendritic layers of the CA1 region and in somata of pyramidal cells in the *stratum pyramidale*. The dendritic compartments analysed were the main dendritic shaft (apical dendrites), spiny branchlets (oblique dendrites) and dendritic spines. Oblique dendrites were identified based on their small diameter and the presence of at least one emerging spine from the dendritic shaft. Dendritic spines were considered as such if: (i) they emerged from a dendritic shaft or (ii) they opposed an axon terminal. Axon terminals were identified based on: (i) the concave shape of the P-face and the accumulation of intramembrane particles (IMPs) on the opposing exoplasmic-face (E-face) of a spine or dendrite; or (ii) the presence of synaptic vesicles on their cross-fractured portions. Non-specific background labeling was measured on E-face structures surrounding the measured P-faces. Images of the identified compartments were selected randomly over the entire dendritic tree of CA1 pyramidal cells and then captured with an ORIUS SC1000 CCD camera (Gatan, Munich, Germany). The area of the selected profiles and the number of immunoparticles were measured using our GPDQ software (33). Immunoparticle densities were presented as mean ± SEM between animals. Statistical comparisons were performed with GraphPad Prism 5 software (La Jolla, CA, USA).

Number of $GABA_{B1}$ immunoparticles in clusters along the membrane surface

To determine the number of $GABA_{B1}$ immunoparticles composing the clusters that are present in different compartments of CA1 pyramidal cells in the two genotypes (wild type and APP/PS1) and the three ages (1, 6 and 12-months), we used the same set of images for the above analysis and the GPDQ software. The software reports the number of particles, their area (as the area inside the convex hull of the particles in the cluster) or the distance to the nearest cluster of particles. By default, the software uses the minimum number of particles in a cluster fixed to three, so all clusters with one or two particles are discarded. More information in all parameters that need to be set in the software is detailed elsewhere (33). The data were expressed as the percentage of clusters with distinct number of immunoparticles per cluster, in different compartments both in wild-type and APP/PS1 mice.

Quantification and analysis of pre-embedding immunogold data

To establish the relative abundance of $GABA_{B1}$ immunoreactivity in different compartments of CA1 pyramidal cells between the two genotypes (wild type and APP/PS1) and the three ages (1, 6 and 12-months), we used 60-µm-thick coronal slices processed for pre-embedding immunogold immunohistochemistry. The procedure was similar to that used previously (34). Briefly, for each of three adult animals, three samples of tissue were obtained for the preparation of embedding blocks, thus using in total nine blocks. To minimize false negatives, electron microscopic serial ultrathin sections were cut close to the surface of each block, as immunoreactivity decreased with depth. We estimated the quality of immunolabeling by always selecting the areas with optimal gold labeling at approximately the same distance from the cutting surface. Randomly selected areas were then photographed from the selected ultrathin sections and used with final magnification between 30 000 and 50 000×. Quantification of immunogold labeling was carried out in reference areas of the CA1 region totaling approximately 2500 μm^2. We counted immunoparticles identified in each reference area and present in different subcellular compartments: dendritic spines, dendritic shafts and axon terminals. The data were expressed as a percentage of immunoparticles in each subcellular compartment, both in the plasma membrane and at intracellular sites.

Controls

To test method specificity in the procedures for electron microscopy, the primary antibody was either omitted or replaced with 5% (v/v) normal serum of the species of the primary antibody, resulting in total loss of the signal. For the pre-embedding technique, labelling patterns were also compared with those obtained with Calbindin (polyclonal rabbit anti-Calbindin D-9k CB9; Swant, Marly, Switzerland); only the antibodies against $GABA_{B1}$ consistently labeled the plasma membrane. To test method specificity in the procedures for western blots and histoblots, antisera against $GABA_{B1}$ was tested on hippocampal membranes and brain sections, respectively, of $GABA_{B1}$ knockout mice. In our samples, the immunolabeling signal was completely absent in the knockout mice, while a strong signal was present in wild-type mice.

Data analysis

Statistical analyses for morphological data were performed using SigmaStat Pro (Jandel Scientific) and data were presented as mean ± SEM unless indicated otherwise. Statistical significance was defined as $P < 0.05$. The statistical evaluation of the immunogold densities was performed using the two-way ANOVA test and further compared with the Bonferroni *post hoc* test.

RESULTS

Similar brain expression of $GABA_B$ receptors in control and APP/PS1 mice

We first determined whether the $GABA_B$ receptor expression was impaired in the brain of APP/PS1 mice at time points when Aβ deposition is observed. We selected ages with (i) no sign of pathology (1 month; Figure 1A-C), (ii) starting Aβ deposition (6 months; Figure 1D-F) and (iii) cognitive deficits, severe synapse loss and widespread Aβ deposition (12 months; Figure 1G-I). To analyse region-dependent alterations in $GABA_B$ receptor expression in the brain of APP/PS1 and age-matched wild-type mice, we used a $GABA_{B1}$ subunit-specific antibody in conventional histoblots (33).

In the brain, the overall expression of $GABA_{B1}$ revealed marked region-specific differences at all ages analysed, with very similar expression patterns in wild type and APP/PS1 mice (Figure 1A-I). In wild-type mice of the three ages analyzed, immunoreactivity for $GABA_{B1}$ was widely distributed in the brain, with strongest immunoreactivities in the cerebellum and thalamus, moderate labeling in the hippocampus, cortex and septum and weak labeling in the caudate putamen and midbrain nuclei, including the inferior and superior colliculi (Figure 1A,D,G). This expression pattern was very similar in the brain of APP/PS1 mice at 1 (Figure 1B), 6 (Figure 1E) and 12 months (Figure 1H) of age. Quantitative analyses was performed to compare the protein densities for 1, 6 and 12 months of age revealed that $GABA_{B1}$ expression levels were similar between wild-type and APP/PS1 mice (Figure 1C,F,I).

Similar hippocampal expression of $GABA_B$ receptors in control and APP/PS1 mice

We next focused on the hippocampus, considered as one of the most vulnerable brain regions affected in AD (56, 57) and explored the laminar expression pattern of $GABA_B$ receptors. Using the histoblot technique, we observed that $GABA_{B1}$ was widely expressed in all hippocampal subfields and dendritic layers at the three ages of wild-type and APP/PS1 mice (Figure 2A-I). In the CA1 region of wild-type

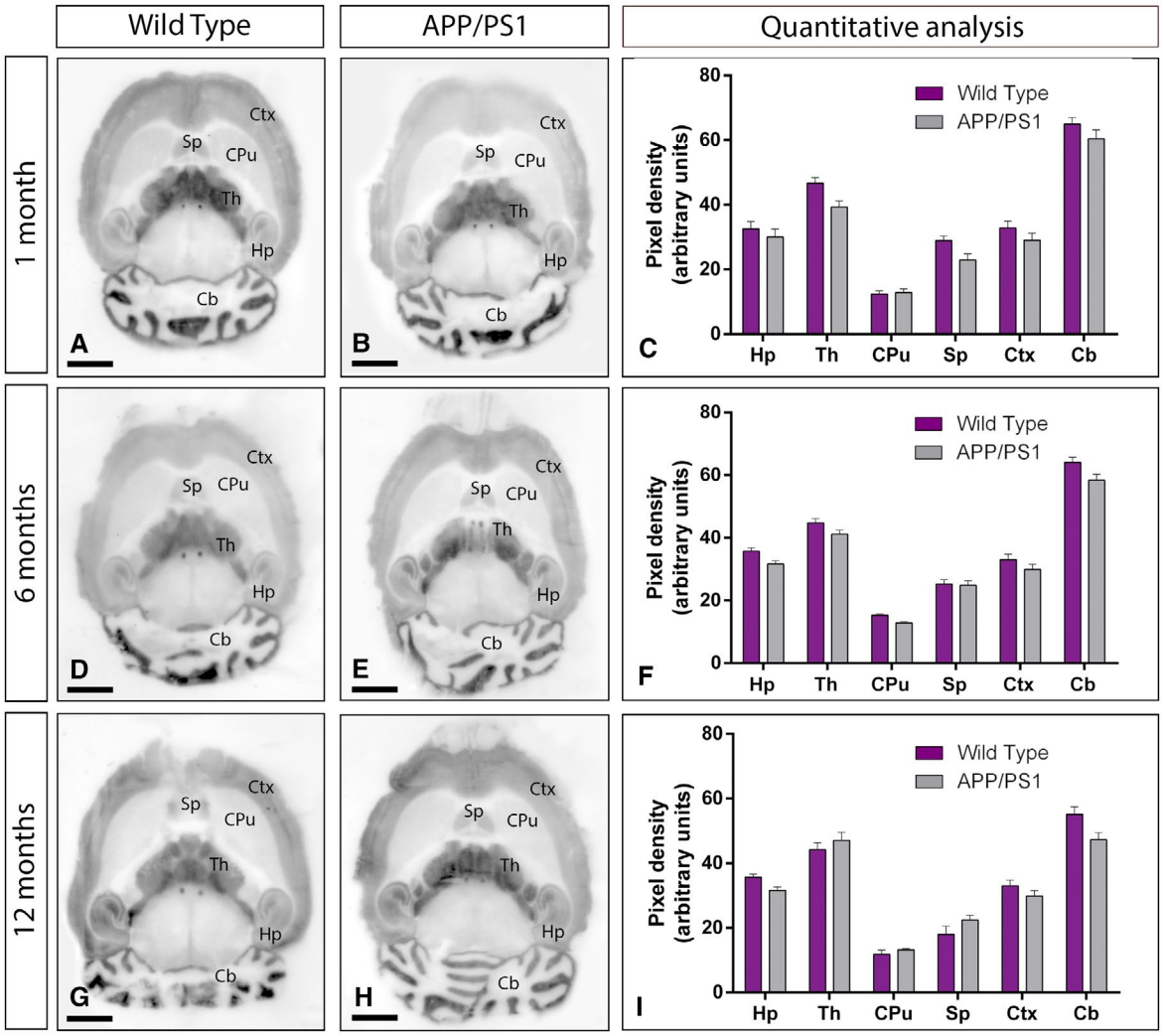

Figure 1. *Regional expression of $GABA_{B1}$ in the brain in wild-type and APP/PS1 mice.* **A-I.** The expression of the $GABA_{B1}$ protein was visualized in histoblots of horizontal brain sections at 1, 6 and 12 months of age in wild-type and APP/PS1 mice using an affinity-purified anti-$GABA_{B1}$ antibody. $GABA_{B1}$ expression in different brain regions was determined by densitometric analysis of the scanned histoblots (panels **C**, **F** and **I**). The strongest $GABA_{B1}$ expression was detected in the cerebellum (Cb) and thalamus (Th), with moderate expression in the hippocampus (Hp), cortex (Ctx) and septum (Sp). The weakest expression level was detected in the caudate putamen (CPu). Densitometric analysis showed no differences in $GABA_{B1}$ expression in APP/PS1 mice compared to age-matched wild type controls. Error bars indicate SEM. Scale bars: 0.2 cm.

mice, at 1, 6 and 12 months of age, $GABA_{B1}$ expression was moderate to strong, with the *strata oriens* and *radiatum* showing the lowest and the *stratum lacunosum-moleculare* showing the highest expression levels (Figure 2A,D,G). The CA3 region of wild-type mice exhibited higher $GABA_{B1}$ expression level than the CA1 region, with *the stratum lacunosum-moleculare* showing the highest expression level within the hippocampus, followed by the *stratum radiatum* (Figure 2A,D,G). The *stratum lucidum* showed weak expression level throughout (Figure 2A,D,G). In the dentate gyrus of wild type, $GABA_{B1}$ immunostaining was weak in the hilus and moderate in the molecular layer (Figure 2A,D,G). The *stratum pyramidale* of the CA1 and CA3 regions and the granule cell layer of the dentate gyrus showed the weakest $GABA_{B1}$ expression (Figure 2A,D,G). The expression pattern of wild-type mice was similar to that of APP/PS1 mice at 1 (Figure 2B), 6 (Figure 2E) and 12 months (Figure 2H) of age. Quantitative analyses of protein densities performed at the three ages confirmed that the expression levels of $GABA_{B1}$ in all subfields and dendritic layers analysed was unchanged between wild-type and APP/PS1 mice (Figure 2C,F,I).

To corroborate the above histoblot data, we further evaluated the expression of $GABA_{B1}$ in the hippocampus using western blot. The mouse pan anti-$GABA_{B1}$ subunit antibody revealed two immunoreactive products with estimated molecular masses of 130 and 100 kDa (Figure 2J), corresponding to the $GABA_{B1a}$ and to the $GABA_{B1b}$ proteins, respectively (25). Since $GABA_{B1a}$ and $GABA_{B1b}$ subunits show a differential compartmentalization in hippocampal neurons (53), both subunits were quantified. The levels of $GABA_{B1a}$ and $GABA_{B1b}$ subunit proteins were unchanged in APP/PS1 compared to age-matched wild-type mice (Figure 2J,K). As

a control, to validate the specificity of the immunoreactions, $GABA_{B1}$ knockout (KO) mice (18) were used. The pattern of immunolabeling for $GABA_{B1}$ observed in the brain of wild-type mice using western blots and histoblots was completely missing in that of the corresponding $GABA_{B1}$ knockout mice ($GABA_{B1}$ -/- brains) (Figure 2L,M), thus demonstrating the specificity of the antibody.

Similar cellular distribution of $GABA_B$ receptors in control and APP/PS1 mice

Given the similar laminar expression of $GABA_{B1}$ in the hippocampus at the three ages analysed, we next sought to investigate the cellular distribution of the receptor at 12 months of age, using light microscopy immunohistochemical techniques. Both in wild-type and APP/PS1 mice,

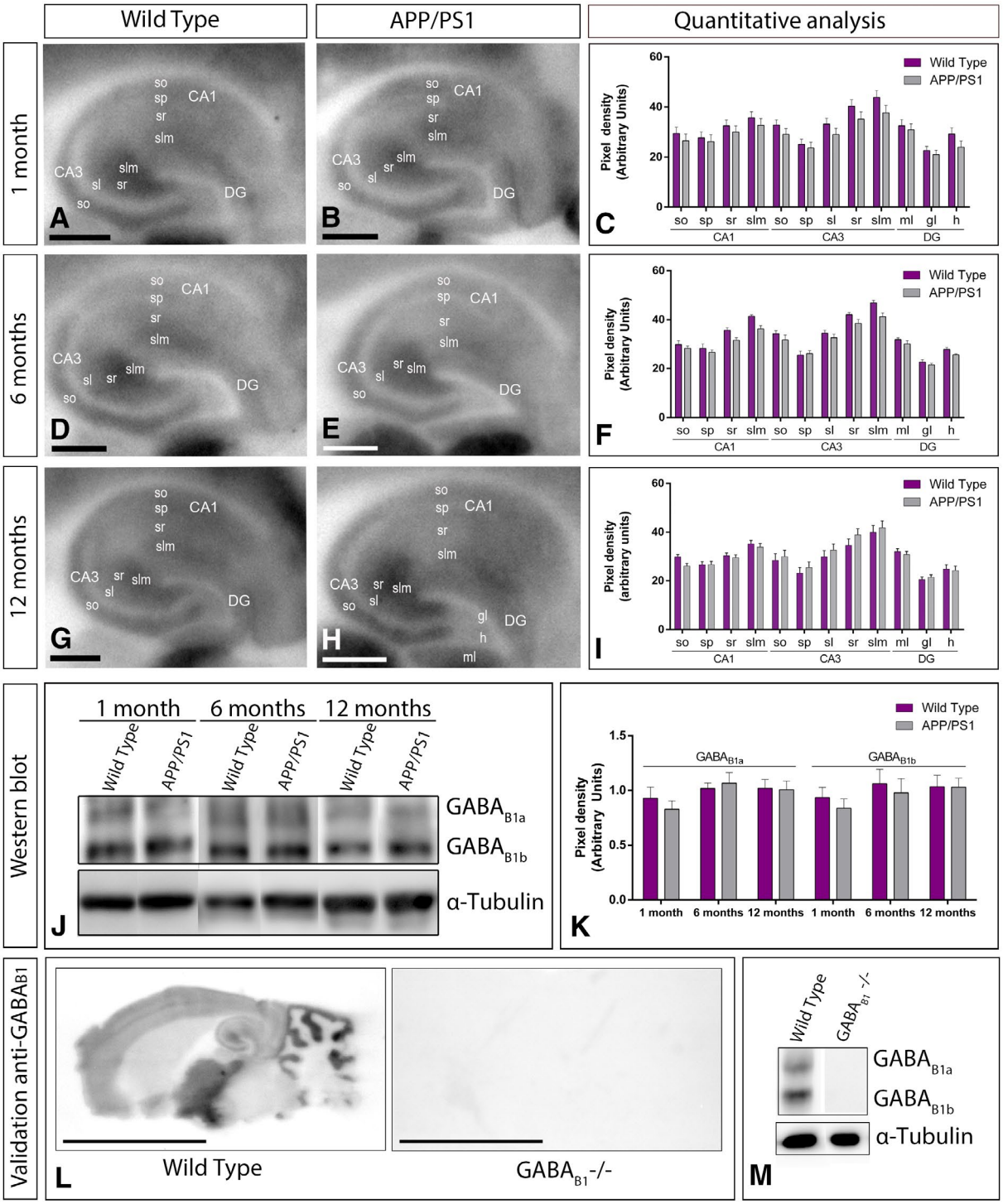

Figure 2. *Hippocampal expression and distribution of $GABA_{B1}$ in wild-type and APP/PS1 mice.* **A-I**. The expression of the $GABA_{B1}$ protein was visualized in histoblots of horizontal brain sections at 1, 6 and 12 months of age in wild-type and APP/PS1 mice using an affinity-purified anti-$GABA_{B1}$ antibody. $GABA_{B1}$ expression in different hippocampal subfields and dendritic layers was determined by densitometric analysis of the scanned histoblots. $GABA_{B1}$ expression was moderate to strong in all dendritic layers of the CA1 and CA3 region and dentate gyrus, with the *stratum lacunosum-moleculare* (slm) of CA3 showing the highest expression level. Densitometric analysis showed no differences in $GABA_{B1}$ expression in APP/PS1 mice compared to age-matched wild type controls. **J,K**. Western blots showing the expression of the $GABA_{B1}$ protein in the hippocampus at 1, 6 and 12 months of age in wild-type and APP/PS1 mice. Crude membrane preparations were subjected to 7.5% SDS-PAGE, transferred on to polyvinylidene difluoride membranes. They were reacted with an anti-pan $GABA_{B1}$ antibody, which recognised both $GABA_{B1a}$ and $GABA_{B1b}$ subunits with estimated molecular masses of 130 and 100 kDa, respectively. The developed immunoblots were scanned and densitometric measurements from five independent experiments were averaged together to compare the protein densities for each age and experimental group. Quantification of $GABA_{B1a}$ and $GABA_{B1b}$ normalised to α-tubulin and expressed as pixel density showed no differences in APP/PS1 mice compared to age-matched wild type controls. Error bars indicate SEM. **L,M**. Characterization of the monoclonal anti-$GABA_{B1}$ in the mouse brain. The pattern of $GABA_{B1}$ expression observed in the wild type using histoblot disappeared completely in the brain of $GABA_{B1}$ null mice ($GABA_{B1}$-/-). Using western blots, immunolabeling signal was abolished in the $GABA_{B1}$-/- mice, while strong bands for $GABA_{B1a}$ and $GABA_{B1b}$ subunits were present in the wild type. Scale bars: **A,B,D,E,G,H**, 0.05 cm; **L**, 0.5 cm.

immunoreactivity for $GABA_{B1}$ in the CA1 and CA3 regions was the highest in the *stratum lacunosum-moleculare* and weaker in the *strata oriens* and *radiatum* (Figure 3A-H). In the dentate gyrus, immunoreactivity for $GABA_{B1}$ was strongest in the molecular layer and weakest in the hilus (Figure 3A-H). In the *stratum pyramidale* of the CA1 and CA3 regions and the granule cell layer of the dentate gyrus immunoreactivity for $GABA_{B1}$ was weakest in the hippocampus, but again very similar between wild-type and APP/PS1 mice (Figure 3C-H). At the cellular level, immunoreactivity for $GABA_{B1}$ was observed in somata of CA1 and CA3 pyramidal cells and granule cells in the dentate gyrus, as well as in somata of some interneurons scattered throughout the hippocampus (Figure 3C-H). The accumulation of Aβ was very high throughout the hippocampus and particularly high in the *stratum lacunosum-moleculare* of the CA1 region and all layers of the dentate gyrus compared to age-matched wild-type mice (Figure 3I,J). Regardless of this massive accumulation of Aβ, the cellular distributions for $GABA_{B1}$ were very similar in wild type compared to APP/PS1 mice.

Altered distribution of $GABA_{B1}$ at the plasma membrane of 6 months old APP/PS1 mice

To explore how $GABA_B$ receptors are organized along the plasma membrane of pyramidal cells, as well as their possible alteration in the hippocampus of APP/PS1 mice, the subcellular localization of the receptors was investigated in the CA1 region of hippocampal sections obtained from 1, 6 and 12 months of age wild-type and APP/PS1 mice. We performed highly-sensitive SDS-FRL labeling for $GABA_{B1}$ (33) to accurately visualize the two-dimensional distribution and precisely calculate the membrane surface densities of this subunit. Consistent with previous pre-embedding immunogold labelling studies (27, 32), $GABA_{B1}$ was detected at high densities on the postsynaptic membrane of the entire somato-dendritic compartment of CA1 principal cells (Figures –7).

We initially performed the ultrastructural analysis at 1 month of age (Figure 4A-G), when no sign of pathology is observed in the hippocampus of APP/PS1 mice. Both in wild-type and APP/PS1 mice, immunoparticles for $GABA_{B1}$ were detected in dendritic spines, dendritic shafts and somata (Figure 4A-I). In all neuronal compartments of CA1 pyramidal cells, immunoparticles for $GABA_{B1}$ were mostly found forming clusters, defined as an aggregation of more than three gold particles and less frequently scattered or isolated single gold particle (Figure 4A-I). The subcellular distribution pattern and intensity of $GABA_{B1}$ labeling observed in wild type at 1 month of age (Figure 4A-E) was similar to that found in APP/PS1 at the same age (Figure 4F-I). Virtually no labeling was observed on the E-face or on cross-fractures (Figure 4A-I). Next, we performed a quantitative comparison of the $GABA_{B1}$ densities in 11 different somato-dendritic compartments in the CA1 region (Figure 4J). Our data revealed a similar graded increase in the density of $GABA_{B1}$ immunoparticles from the soma to the dendritic spines, but more importantly demonstrated similar $GABA_{B1}$ densities along CA1 pyramidal cells in wild-type and APP/PS1 mice (Figure 4J). Altogether, our data show that the membrane surface localization of $GABA_{B1}$ did not change in 1 month old APP/PS1 mice compared to wild type controls.

Next, we performed the ultrastructural analysis at 6 months of age (Figure 5A-H), when Aβ deposition in APP/PS1 mice is accumulating in the hippocampus. In wild-type and APP/PS1 mice, immunoparticles for $GABA_{B1}$ were detected in dendritic spines, dendritic shafts and somata, most frequently forming clusters and less frequently showing a scattered isolated distribution (Figure 5A-H). The subcellular distribution of $GABA_{B1}$ immunogold labeling observed at 6 months of age was similar in wild-type and APP/PS1 mice (Figure 5A-H). Virtually no labeling was observed on the E-faces or on cross-fractures (Figure 5A-H). Quantitative comparison of the $GABA_{B1}$ densities along the membrane surface of CA1 pyramidal neurons revealed two main findings: 1) a graded increase in the density of $GABA_{B1}$ immunoparticles from the soma to the dendritic spines, and 2) similar $GABA_{B1}$ densities along CA1 pyramidal cells in wild-type and APP/PS1 mice, with exception of the *stratum lacunosum-moleculare*, where the $GABA_{B1}$ density varied substantially between wild-type and APP/PS1 mice (Figure 5I). Indeed, our analysis demonstrated the labeling intensity was significantly reduced

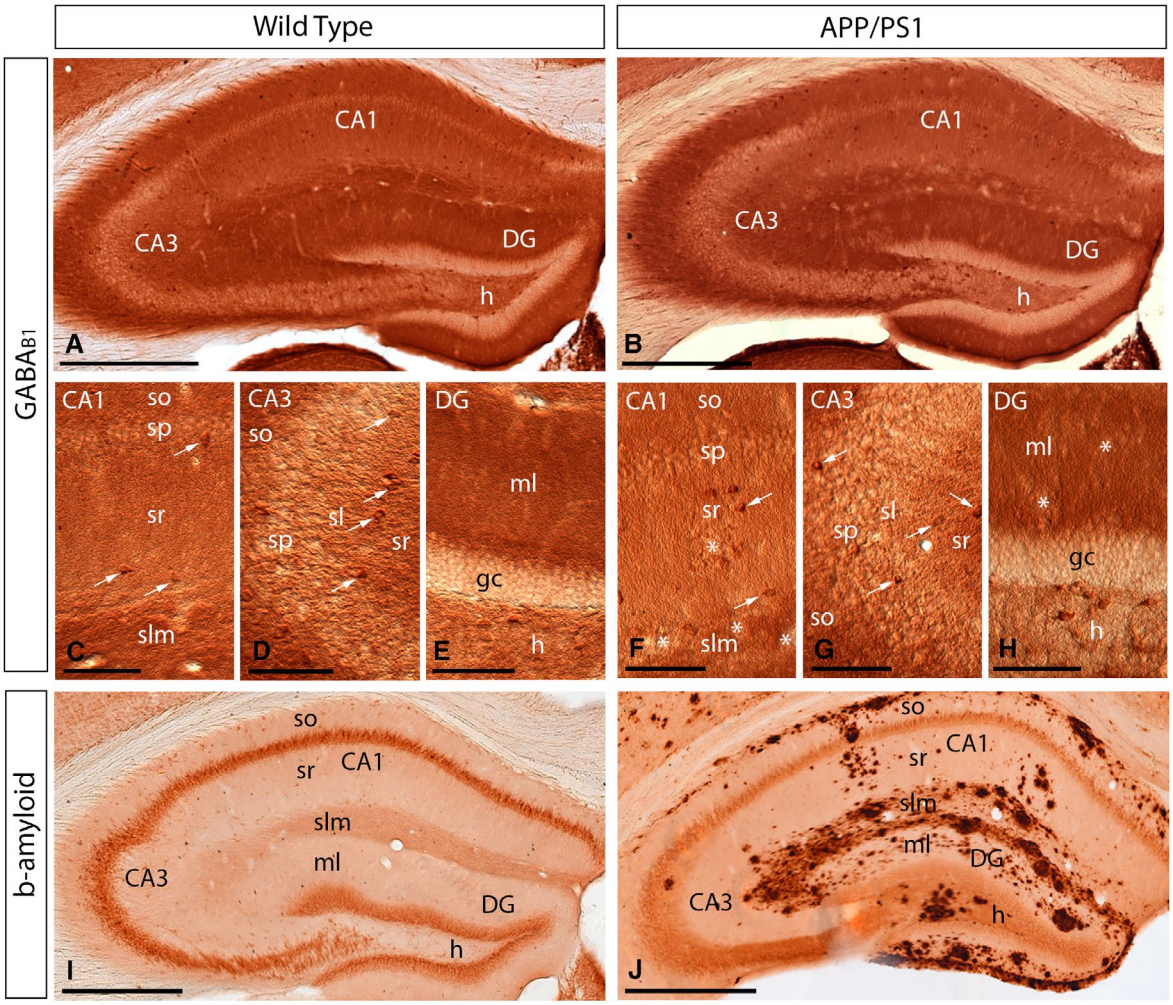

Figure 3. *Regional and cellular distribution of $GABA_{B1}$ in wild-type and APP/PS1 mice.* **A-H**. Immunoreactivity for $GABA_{B1}$ in the hippocampus of wild-type and APP/PS1 mice at 12 months of age using a pre-embedding immunoperoxidase method at the light microscopic level. In the CA1 and CA3 regions and dentate gyrus (DG), $GABA_{B1}$ immunoreactivity was very similar both in the wild-type and the APP/PS1 mice, regardless of accumulation of amyloid plaques (asterisks). Labeling for $GABA_{B1}$ showed the highest intensity in the *stratum lacunosum-moleculare* (slm) and molecular layer (ml) and weaker in the *strata oriens* (so) and *radiatum* (sr). Immunoreactivity for $GABA_{B1}$ was also detected in interneurons throughout all layers (white arrows), with similar distribution pattern and labeling intensity in wild-type and APP/PS1 mice. **I,J**. Immunoreactivity for β-amyloid in wild-type and APP/PS1 mice at 12 months of age, showing high accumulation of Aβ throughout all layers of the hippocampus. *Abbreviations*: CA1 region of the hippocampus; CA3, CA3 region of the hippocampus; DG, dentate gyrus; so, *stratum oriens*; sp, *stratum pyramidale*; sr, *stratum radiatum*; slm, *stratum lacunosum-moleculare*; ml, molecular layer; gc, granule cell layer; h, hilus. Scale bars: **A,B,I,J** 200 µm; **C-H**, 100 µm.

in oblique dendrites (oDen) and spines in APP/PS1 mice (oDen = 28.83 ± 3.45 immunoparticles/µm^2, n = 16 dendrites; s = 49.76 ± 8.79 immunoparticles/µm^2, n = 21 spines) compared to age-match wild-type mice (oDen = 64.34 ± 4.86 immunoparticles/µm^2, n = 16 dendrites; s = 101.58 ± 13.93 immunoparticles/µm^2, n = 21 spines) (Two-way ANOVA test and Bonferroni *post hoc* test, $*P < 0.05$; $****P < 0.0001$) (Figure 5I). Altogether, our data at 6 months of age shows that the plasma membrane localization of $GABA_{B1}$ in APP/PS1 is selectively altered in distal dendrites and spines located in the *stratum lacunosum-moleculare*.

Reduction of $GABA_{B1}$ in the plasma membrane of 12 months old APP/PS1 mice

We further investigated the membrane localization of $GABA_B$ receptors in APP/PS1 mice at 12 months of age, when Aβ deposition is large and cognitive deficits and synapse loss are severe (Figure 6A-N). Immunoparticles for $GABA_{B1}$ were detected along the membrane surface of CA1 pyramidal cells in dendritic compartments and cell bodies in wild- type and APP/PS1 mice (Figure 6A-F). In all strata and neuronal compartments of CA1 pyramidal cells, most immunoparticles for $GABA_{B1}$ were found in clusters, with three or more particles and less frequently scattered single gold particles

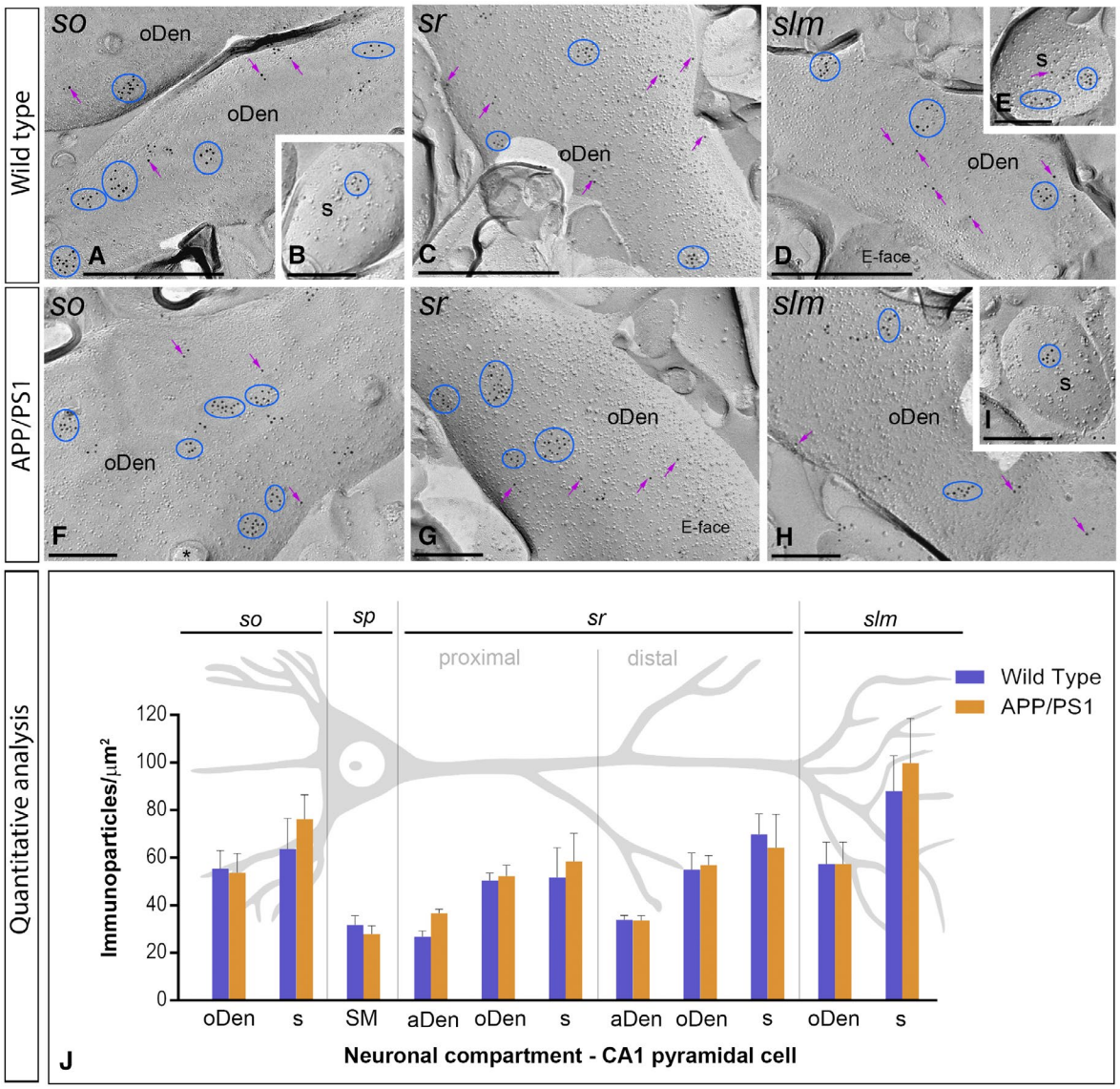

Figure 4. *Subcellular localization of $GABA_{B1}$ in the hippocampus in wild-type and APP/PS1 mice at 1 month.* Electron micrographs obtained from different strata of the CA1 region showing immunoparticles for $GABA_{B1}$ along the membrane surface of pyramidal cells, as detected using the SDS-FRL technique. **A-H**. In wild type and APP/PS1, clusters of $GABA_{B1}$ immunoparticles (blue ellipses/circles) associated with the P-face were detected in dendritic shafts, illustrated here for oblique dendrites (oDen) and dendritic spines (s) of pyramidal cells in all strata of the CA1 region. Lower density of immunoparticles for $GABA_{B1}$ was also detected scattered (purple arrows) outside the clusters. Fractured spine necks are indicated with asterisks (*). The E-face is free of any immunolabeling. **J**. Quantitative analysis of $GABA_{B1}$ immunogold labeling in eleven neuronal compartments. The density gradient of $GABA_{B1}$ immunoparticles along the membrane surface of CA1 pyramidal cells was very similar between wild-type and APP/PS1 mice. Error bars indicate SEM. Abbreviations: *so*, *stratum oriens*; *sp*, *stratum pyramidale*; *sr*, *stratum radiatum*; *slm*, *stratum lacunosum-moleculare*; aDen, apical dendrite; oDen, oblique dendrite; s, spine; SM, soma. Scale bars: **A**,**C**,**D**, 0.5 µm; **B**,**E-I**, 0.2 µm.

outside the clusters (Figure 6A-F). No labeling was observed on the E-face or on cross-fractures (Figure 6A-F). In APP/PS1 mice, $GABA_{B1}$ immunoparticles were observed in all strata in the CA1 region, but their distribution pattern changed significantly. Thus, both fewer immunoparticles and fewer clusters were detected along the membrane surface of CA1 pyramidal cells (Figure 6G-N).

Next, we performed a quantitative comparison of the $GABA_{B1}$ densities in somato-dendritic compartments of CA1 pyramidal cells (Figure 7A). This analysis revealed a significant decrease between wild-type and APP/PS1 mice in all strata analyzed (Figure 7A). Altogether, our data shows that the membrane surface localization of $GABA_{B1}$ was reduced significantly in 12-month-old APP/PS1 mice

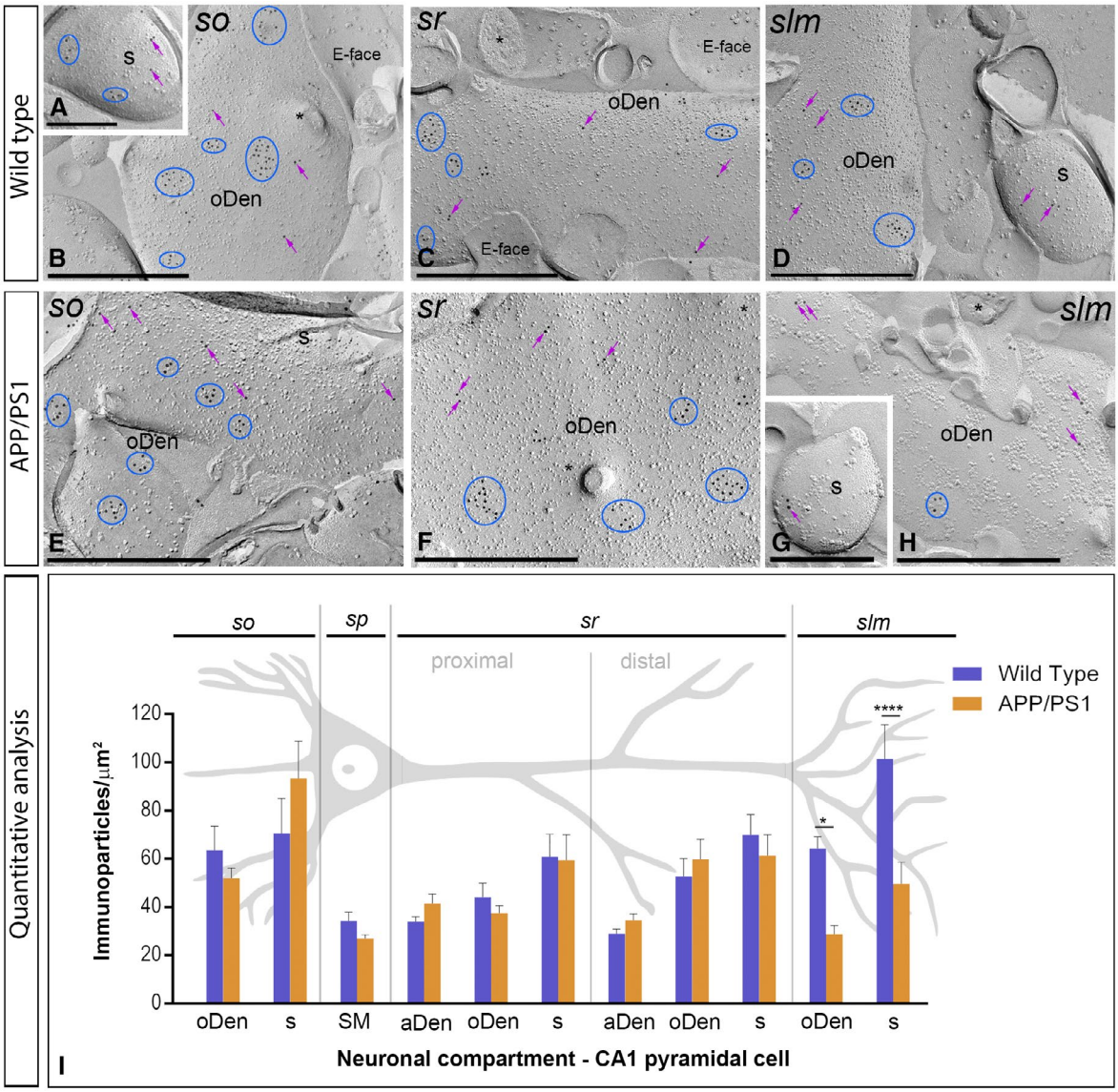

Figure 5. *Subcellular localization of $GABA_{B1}$ in the hippocampus in wild-type and APP/PS1 mice at 6 months.* Electron micrographs obtained from different strata of the CA1 region showing immunoparticles for $GABA_{B1}$ along the membrane surface of pyramidal cells, as detected using the SDS-FRL technique. **A-H**. In wild type and APP/PS1, clusters of $GABA_{B1}$ immunoparticles (blue ellipses/circles) associated with the P-face were detected in dendritic shafts, illustrated here for oblique dendrites (oDen) and dendritic spines (s) of pyramidal cells in all strata of the CA1 region. Lower density of immunoparticles for $GABA_{B1}$ was also detected scattered (purple arrows) outside the clusters. Fractured spine necks and other cross-fractures are indicated with asterisks (*). The E-face is free of any immunolabeling. **I**. Quantitative analysis of $GABA_{B1}$ immunogold labeling in 11 neuronal compartments of CA1 pyramidal cells. The density gradient of membrane surface $GABA_{B1}$ immunoparticles was very similar between wild-type and APP/PS1 mice in all strata except in the *stratum lacunosum-moleculare* (slm), where we found significant differences in both oblique dendrites (WT: 60.27 ± 5.60 immunoparticles/µm²; APP/PS1: 35.37 ± 3.61 immunoparticles/µm²) and dendritic spines (WT: 103.68 ± 18.69 immunoparticles/µm²; APP/PS1: 58.09 ± 13.78 immunoparticles/µm²) (Two-way ANOVA test and Bonferroni *post hoc* test, $*P < 0.05$; $****P < 0.0001$). Error bars indicate SEM. Abbreviations: *so*, *stratum oriens*; *sp*, *stratum pyramidale*; *sr*, *stratum radiatum*; *slm*, *stratum lacunosum-moleculare*; aDen, apical dendrite; oDen, oblique dendrite; s, spine; SM, soma. Scale bars: **A,G**, 0.25 µm; **B-F,H**, 0.5 µm.

(Two-way ANOVA test and Bonferroni *post hoc* test, $*P < 0.05$; $****P < 0.0001$).

Finally, to determine how the reduction in $GABA_{B1}$ density is taking place at the membrane surface of CA1 pyramidal cells in 12-month-old APP/PS1 mice, we analyzed the composition of clusters of $GABA_{B1}$ immunoparticles in dendritic shafts and spines along the membrane surface in the different hippocampal layers. We analyzed neuronal compartments in all strata, but provide only the example of oDen in the proximal and distal parts of the *stratum radiatum* and the *stratum lacunosum-moleculare* (Figure 7B). To avoid differences in the size

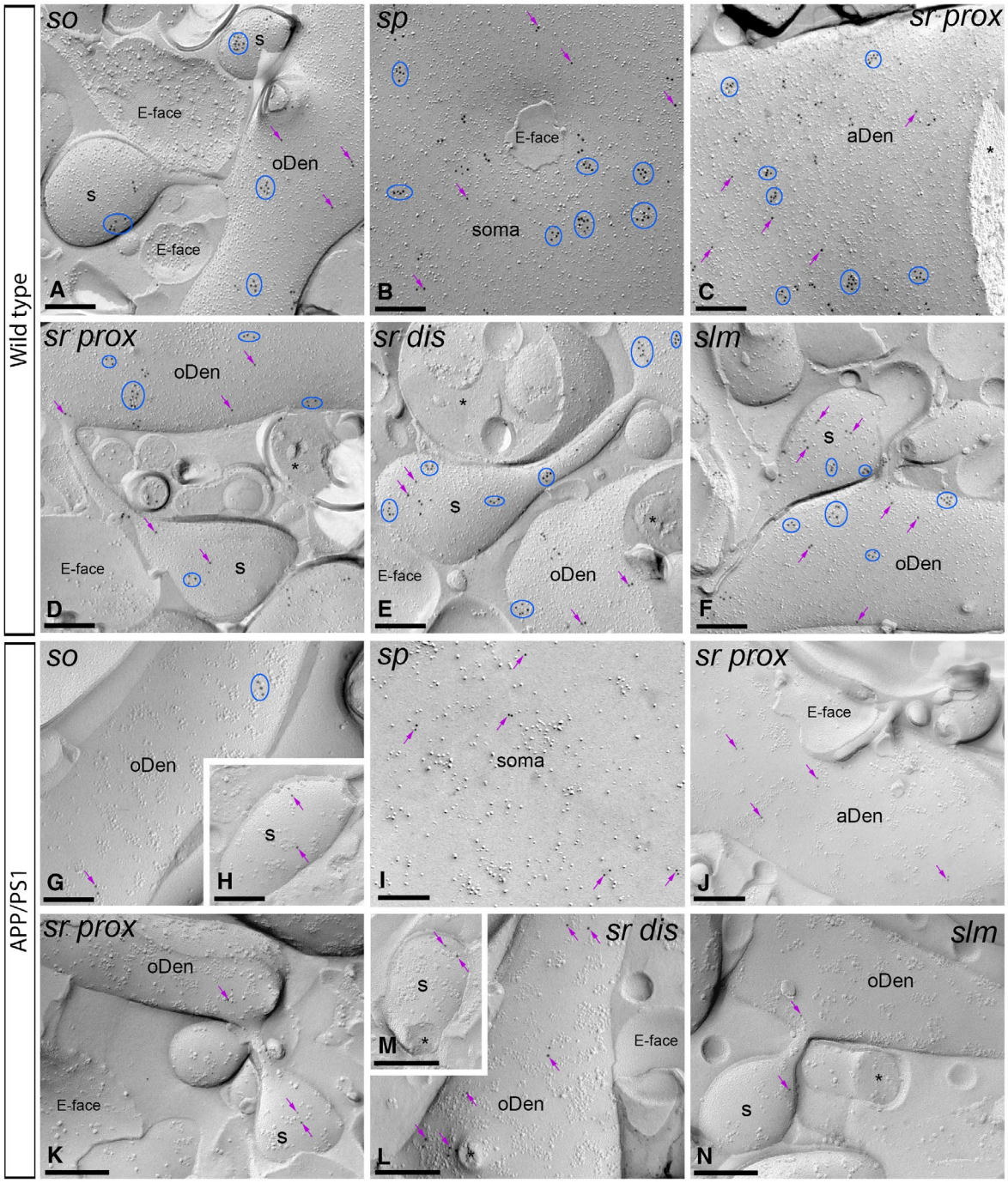

Figure 6. *The density of plasma membrane of $GABA_{B1}$ is reduced in the hippocampus of APP/PS1 mice at 12 months.* Electron micrographs of the CA1 region showing immunoparticles for $GABA_{B1}$ along the membrane surface of pyramidal cells, as detected using the SDS-FRL technique. **A-F**. In wild type, clusters of $GABA_{B1}$ immunoparticles (blue ellipses/circles) associated with the P-face were detected in dendritic shafts, illustrated here for oblique dendrites (oDen) and dendritic spines (s) of pyramidal cells in all strata of the CA1 region. Lower density of immunoparticles for $GABA_{B1}$ was also detected scattered (purple arrows) outside the clusters. **G-N**. In APP/PS1, surface $GABA_{B1}$ immunoparticles were detected in the P-face of all compartments of CA1 pyramidal cells. However, $GABA_{B1}$ immunoparticles were detected at lower frequency forming clusters (blue ellipses/circles), being showing a scattered distribution (purple arrows). Fractured spine necks and other cross-fractures are indicated with asterisks (*). The E-face is free of any immunolabeling. Scale bars: **A-N**, 0.2 μm.

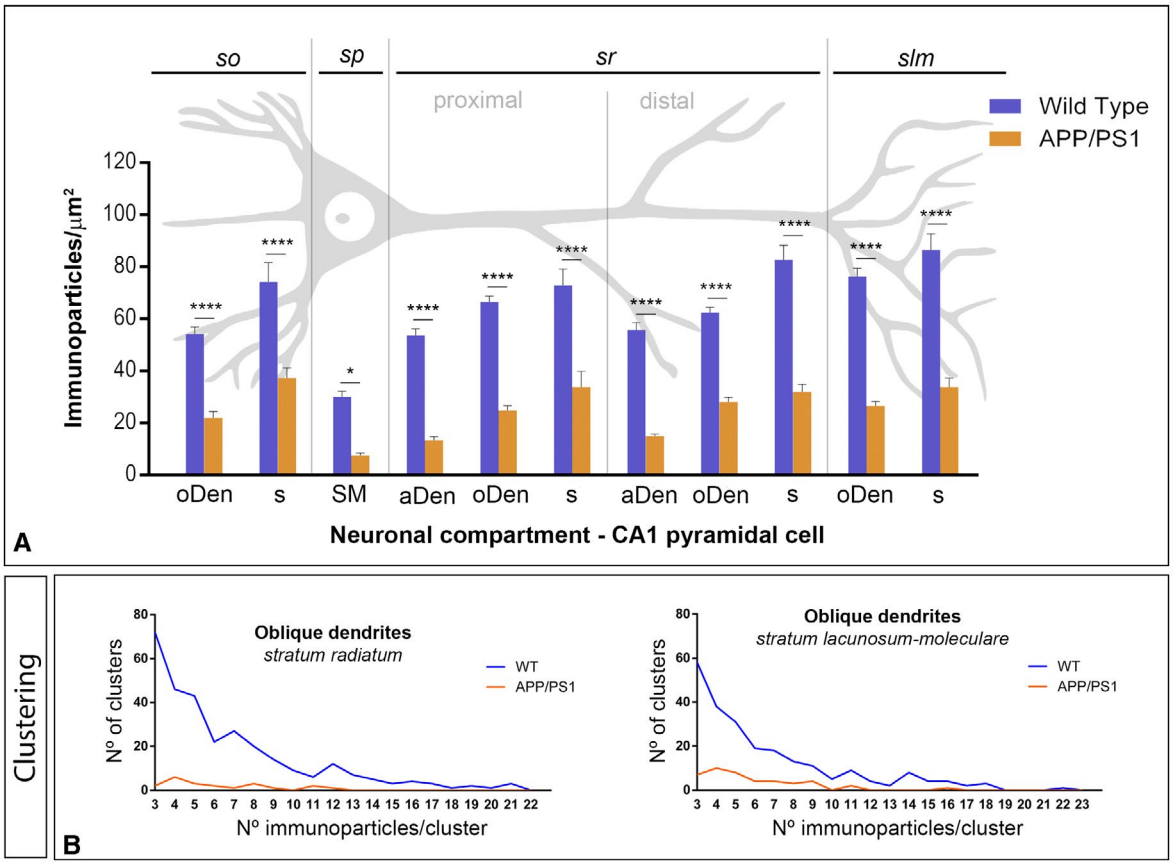

Figure 7. *Density gradient of $GABA_{B1}$ immunoparticles along the* membrane surface *of CA1 pyramidal cells in wild type and APP/PS1 mice at 12 months.* **A**. Quantitative analysis of $GABA_{B1}$ immunogold labeling in eleven neuronal compartments of CA1 pyramidal cells. The density gradient of membrane surface $GABA_{B1}$ immunoparticles was significantly reduced in the APP/PS1 mice compared to age-matched wild type controls in all strata and compartments analyzed Two-way ANOVA test and Bonferroni *post hoc* test, $*P < 0.05$; $****P < 0.0001$). Error bars indicate SEM. Abbreviations: *so*, *stratum oriens*; *sp*, *stratum pyramidale*; *sr*, *stratum radiatum*; *slm*, *stratum lacunosum-moleculare*; aDen, apical dendrite; oDen, oblique dendrite; s, spine; SM, soma. **B**. Quantitative analysis showing composition of clusters of $GABA_{B1}$ immunoparticles along the membrane surface in the *strata radiatum* and *lacunosum-moleculare* in wild-type and APP/PS1 mice at 12 months on age in oblique dendrites. In the two dendritic layers analyzed, the number and size of clusters of $GABA_{B1}$ immunoparticles was reduced in the APP/PS1 mice (68 clusters with a range of 3 to 12 immunoparticles in the *sr*; 60 clusters with a range of 3 to 13 immunoparticles in the *slm*) compared to age-matched wild type controls (298 clusters with a range of 3 to 21 immunoparticles in the *sr*; 230 clusters with a range of 3 to 22 immunoparticles in the *slm*).

of dendrites present in each EM picture analyzed or dendritic alterations induced by AD, we performed this analysis in a similar total area (140.00 μm^2) of oDen. In the proximal part of the *stratum radiatum*, we detected a total of 68 clusters with a range of 3 to 12 immunoparticles in APP/PS1 mice, while detected 298 clusters with a range of 3 to 29 immunoparticles for $GABA_{B1}$ in wild-type mice (Figure 7B). In the distal part of the *stratum radiatum*, we detected a total of 57 clusters with a range of 3 to 12 immunoparticles in APP/PS1 mice, while detected 204 clusters with a range of 3 to 29 immunoparticles for $GABA_{B1}$ in wild-type mice (Figure 7B). Similarly, in the *stratum lacunosum-moleculare*, we detected a total of 60 clusters with a range of 3 to 13 immunoparticles in APP/PS1 mice, while we detected 234 clusters with a range of 3 to 37 immunoparticles for $GABA_{B1}$ in wild-type mice (Figure 7B). Altogether, the analysis showed that the number and the size of clusters of $GABA_{B1}$ immunoparticles were reduced in the two dendritic layers in the APP/PS1 mice.

Reduction in the density of presynaptic $GABA_{B1}$ in 12-month-old APP/PS1 mice

Immunoparticles for $GABA_{B1}$ were not only confined to somato-dendritic domains of CA1 pyramidal cells, but also present in axon terminals, as previously reported (27, 32). Thus, we further investigated whether the localization of $GABA_{B1}$ at presynaptic sites is altered in the hippocampus of APP/PS1 (Figure 8), paralleled to the decrease found in somato-dendritic compartments at 12 months of age. We performed SDS-FRL labeling for $GABA_{B1}$ to unravel its membrane surface densities in the *strata radiatum* and *lacunosum-moleculare* of the CA1 region. In wild-type

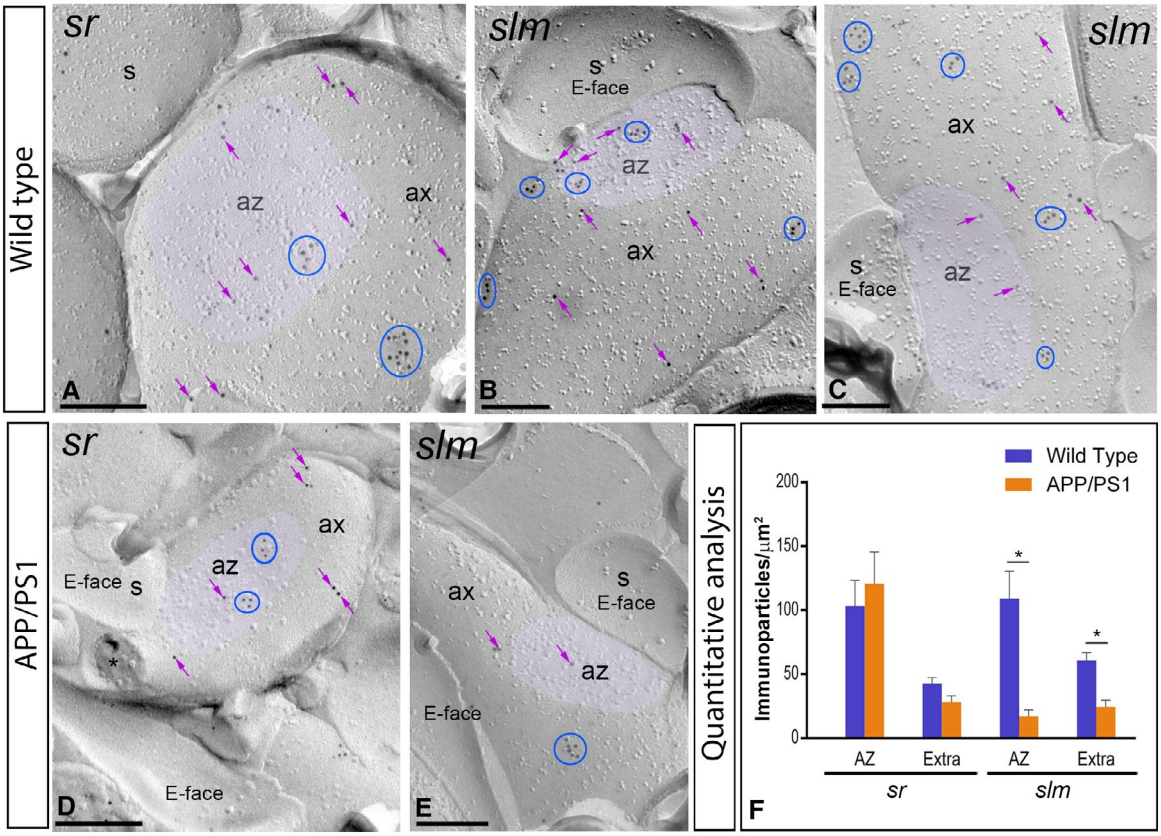

Figure 8. *Presynaptic localization of $GABA_{B1}$ in the hippocampus in wild-type and APP/PS1 mice.* Electron micrographs showing immunoparticles for $GABA_{B1}$ in presynaptic compartments in the *strata radiatum* (*sr*) and *lacunosum-moleculare* (*slm*) of the CA1 region of the hippocampus at 12 months of age, as detected using the SDS-FRL technique. **A-C**. In wild type, immunoparticles for $GABA_{B1}$ were found within the active zone (az, purple overlay), recognized by the concave shape of the P-face and the accumulation of IMPs, and along the extrasynaptic site of axon terminals (ax), forming clusters (blue ellipses/circles) and also detected scattered (purple arrows) outside the clusters. **D,E**. In APP/PS1, fewer immunoparticles for $GABA_{B1}$, forming clusters (blue ellipses/circles) or scattered (purple arrows), were detected within the active zone (az, purple overlay) and along the extrasynaptic plasma membrane of axon terminals (ax). Cross-fractures are indicated with asterisks (*). **F**. Densities of immunoparticles for $GABA_{B1}$ in presynaptic compartments in the *sr* and *slm* in wild-type and APP/PS1 mice. No differences were detected in densities of $GABA_{B1}$ immunoparticles in the *sr* (WT: AZ = 103.31 ± 20.16 immunoparticles/µm^2 and Extra = 42.97 ± 4.47 immunoparticles/µm^2; APP: AZ = 120.95 ± 24.58 immunoparticles/µm^2; Extra = 28.08 ± 4.96 immunoparticles/µm^2), but significant differences were detected in the *slm* (WT: AZ = 109.03 ± 21.62 immunoparticles/µm^2 and Extra = 60.79 ± 6.11 immunoparticles/µm^2; APP: AZ = 17.32 ± 4.99 immunoparticles/µm^2; Extra = 24.64 ± 5.17 immunoparticles/µm^2) (Two-way ANOVA test and Bonferroni *post hoc* test, $*P < 0.05$). Error bars indicate SEM. Scale bars: **A-E**, 0.2 µm.

animals, immunoparticles for $GABA_{B1}$ were detected within the active zone of axon terminals, identified by the concave shape of the P-face and the accumulation of IMPs (23) and along the extrasynaptic site of axon terminals (Figure 8A-C). $GABA_{B1}$ immunoparticles were detected both forming clusters and scattered outside the clusters, both in the active zone and at the extrasynaptic sites (Figure 8A-C). The density of $GABA_{B1}$ immunoparticles was higher at the active zones (AZ; *sr* = 103.31 ± 20.16 immunoparticles/µm^2, n = 82 particles; *slm* = 109.03 ± 21.62 immunoparticles/µm^2, n = 149 particles) than at the extrasynaptic sites (Extra; *sr* = 42.97 ± 4.47 immunoparticles/µm^2, n = 305 particles; *slm* = 60.79 ± 6.11 immunoparticles/µm^2, n = 347 particles) (Figure 8F). In APP/PS1 animals, $GABA_{B1}$ immunoparticles were detected in the same presynaptic compartments also showing larger density at the active zone terminals than at extrasynaptic sites, showing clusters and scattered distributions (Figure 8D-E). However, quantitative comparisons with age-matched wild-type mice did not show differences in the density of $GABA_{B1}$ immunoparticles in the *sr* (AZ = 120.95 ± 24.58 immunoparticles/µm^2, n = 79 particles; Extra = 28.08 ± 4.96 immunoparticles/µm^2, n = 81 particles) (Two-way ANOVA test and Bonferroni *post hoc* test, p = 0.68), while we found significant differences in the *slm* (AZ = 17.32 ± 4.99 immunoparticles/µm^2, n = 19 particles; Extra = 24.64 ± 5.17 immunoparticles/µm^2, n = 67 particles) (Two-way ANOVA test and Bonferroni *post hoc* test, $*P < 0.05$) (Figure 8F).

To test the consistency and specificity on the reduction of $GABA_B$ receptors in the APP/PS1 mice described above, as control of our technical approach and mouse model we analysed the distribution of four different proteins:

(i) AMPA receptors, known to localise in excitatory synapses in an activity-dependent manner (Supplementary Figure S1); (ii) the GluN1 subunit of NMDA receptors, which are not incorporated in an activity-dependent manner into synapses (Supplementary Figure S2); (iii) the GIRK2 subunit of G protein-gated inwardly rectifying potassium channels, which are known effector ion channels of $GABA_B$ receptors (Supplementary Figure S2); and (iv) the synaptosomal-associated protein SNAP-25, which is responsible for the Ca^{2+}-dependent exocytosis of neurotransmitters, thus playing a key role to normal functioning of brain (Supplementary Figure S2). Thus, using the SDS-FRL method, we determined the densities of the four proteins receptors at synapses of the *stratum lacunosum-moleculare* (the subfield in which we detected most alteration in the localization of $GABA_B$ receptors) in the CA1 region of hippocampal sections. In APP/PS1 mice, compared to control mice, lower density of immunoparticles for AMPA (Supplementary Figure S1) and NMDA (Supplementary Figure S2) were detected in excitatory synapses of dendritic spines, fewer immunoparticles for GIRK2 (Supplementary Figure S2) were detected in dendritic shafts and spines of pyramidal cells and fewer immunoparticles for SNAP-25 (Supplementary Figure S2) were detected in axon terminals establishing excitatory synapses with dendritic spines. These reductions, which are in agreement with the current literature, validate the effect described for $GABA_B$ receptors.

Increase of $GABA_{B1}$ in the cytoplasm of CA1 pyramidal cells and axon terminals in APP/PS1 mice

We next sought to investigate why the localization of $GABA_{B1}$ in the membrane surface of CA1 pyramidal cells and axon terminals is significantly reduced in the hippocampus of APP/PS1 at 12 months of age when the total amount of protein remains invariable, as shown by histoblots and western blots. To explore possible receptor internalization and accumulation in intracellular domains of CA1 pyramidal cells and axon terminals of APP/PS1 mice compared to age-matched wild type controls, the subcellular localization of $GABA_{B1}$ was investigated at 1, 6 and 12 months of age. We used the pre-embedding immunogold technique and quantitative analysis on tissue blocks taken from the proximal part of the *stratum radiatum* and the *stratum lacunosum-moleculare* of the CA1 area.

At 1 month of age, immunoreactivity for $GABA_{B1}$ was primarily found along the extrasynaptic plasma membrane of dendritic spines and shafts of CA1 pyramidal cells and also associated at intracellular sites in dendritic spines (Figure 9A,B). Quantitative analysis performed in the *strata radiatum (sr)* and *lacunosum-moleculare (slm)* of the CA1 area showed similar proportion of postsynaptic $GABA_{B1}$ immunoparticles in the plasma membrane vs. intracellular in APP/PS1 (Plasma membrane: 65.52% in *sr* and 65.11% in *slm*; Intracellular: 34.48% in *sr* and 34.89% in *slm*) and age-matched wild-type mice (Plasma membrane: 64.04% in *sr* and 64.68% in *slm*; Intracellular: 35.96% in *sr* and 35.32% in *slm*) (Figure 9C).

At 6 months of age, immunoreactivity for $GABA_{B1}$ followed similar distribution than at 1 month, being also observed along the extrasynaptic plasma membrane and intracellular sites of dendritic spines and shafts of CA1 pyramidal cells (Figure 9D-E). However, quantitative analysis showed some differences in the plasma membrane vs. intracellular between the *stratum radiatum* and the *stratum lacunosum-moleculare* of the CA1 area. Thus, in the *stratum radiatum* we did not detect differences in the total amount of postsynaptic immunoparticles between wild-type and APP/PS1 mice (Plasma membrane: 63.45% in wild type and 63.46% in APP/PS1; Intracellular: 36.55% in wild type and 36.54% in APP/PS1) (Figure 9F). Consistent with this data, similar percentage of immunoparticles were observed in dendritic spines and shafts between wild-type and APP/PS1 mice (Figure 9F). However, we detected changes in the *stratum lacunosum-moleculare* in the plasma membrane vs. intracellular among wild-type and APP/PS1 mice (Plasma membrane: 62.06% in wild type and 41.05% in APP/PS1; Intracellular: 37.94% in wild type and 58.05% in APP/PS1) (Figure 9F).

At 12 months of age, immunoreactivity for $GABA_{B1}$ was again localized along the extrasynaptic plasma membrane of dendritic spines and shafts, as well as associated at intracellular sites in dendritic spines (Figure 9G-I). Quantitative analysis showed clear differences in the plasma membrane vs. intracellular both in the *stratum radiatum* (Plasma membrane: 58.81% in wild type and 32.60% in APP/PS1; Intracellular: 41.19% in wild type and 67.40% in APP/PS1) and the *stratum lacunosum-moleculare* (Plasma membrane: 54.23% in wild type and 15.19% in APP/PS1; Intracellular: 45.77% in wild type and 84.81% in APP/PS1) of the CA1 area. These differences in plasma membrane vs. intracellular were detected in dendritic shafts and spines in the two strata (Figure 9G-I). To clarify the intracellular compartments on which $GABA_{B1}$ is accumulated, we performed double labeling immunofluorescence with different markers (Rab4, EEA1, LAMP1 or CHOP). We found no differences in the co-localization pattern in the APP/PS1 mice compared to age-matched wild type controls with the makers employed (Supplementary Figure S4).

Presynaptically, immunoreactivity for $GABA_{B1}$ was occasionally detected in axon terminals establishing asymmetrical synapses with dendritic spines (Figure 9). At 1 month of age, $GABA_{B1}$ presynaptic labeling was similar between wild-type and APP/PS1 animals (Figure 9C). At 6 months of age, we detected changes in the plasma membrane vs. intracellular among wild type and APP/PS1 in the *stratum radiatum* (Plasma membrane: 57.57% in wild type and 46.30% in APP/PS1; Intracellular: 42.42% in wild type and 53.70% in APP/PS1) and *stratum lacunosum-moleculare* (Plasma membrane: 62.12% in wild type and 39.25% in APP/PS1; Intracellular: 37.88% in wild type and 60.75% in APP/PS1) (Figure 9F). These differences were more pronounced at 12 months of age, detecting changes in the *stratum radiatum* (Plasma membrane: 60.78% in wild type and 33.33% in APP/PS1;

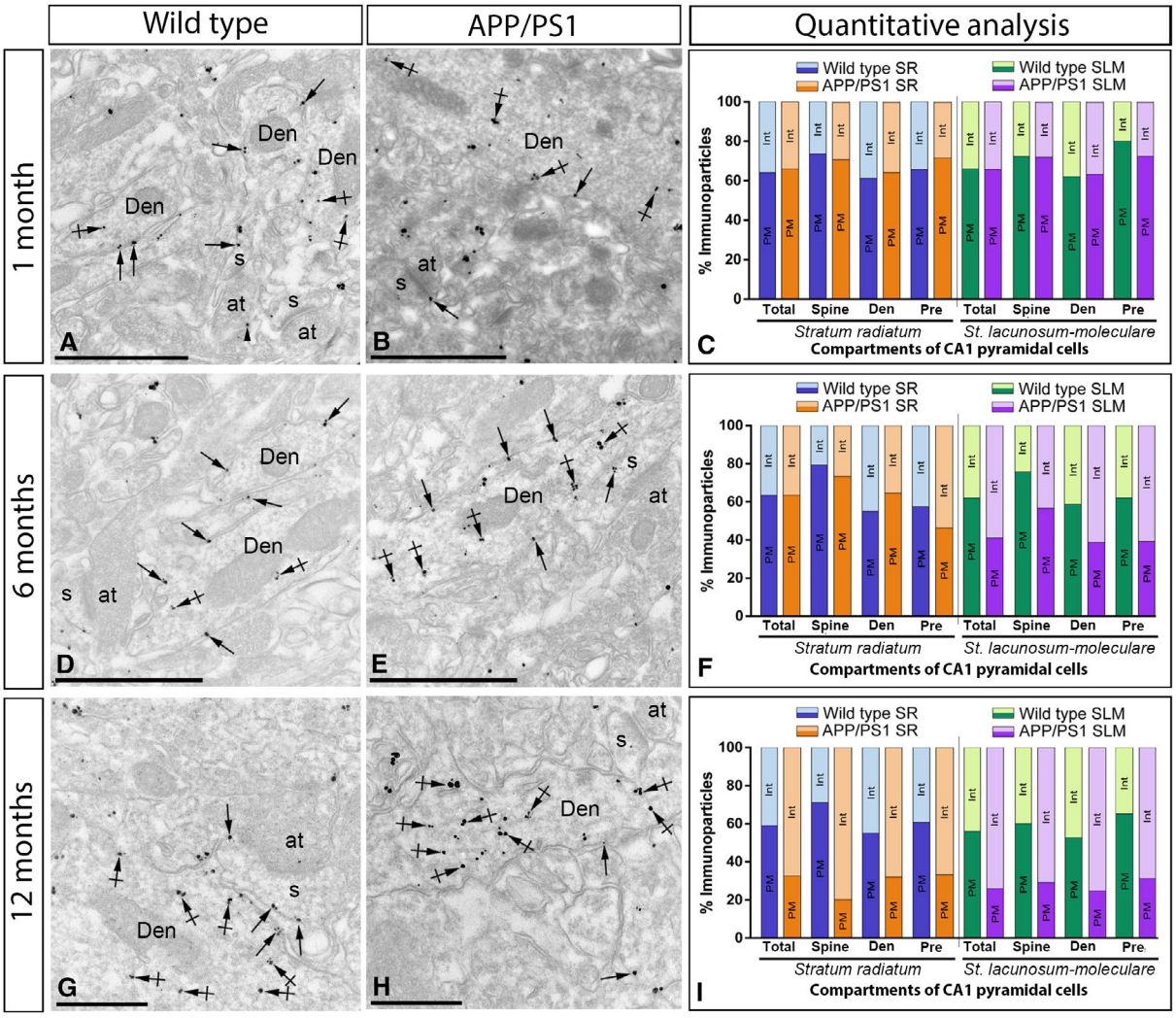

Figure 9. *Intracellular distribution of $GABA_{B1}$ is increased in the hippocampus of APP/PS1 mice.* Electron micrographs showing immunoparticles for $GABA_{B1}$ in pyramidal cells of the CA1 region at 1, 6 and 12 months of age in wild -type and APP/PS1 mice, as detected using a pre-embedding immunogold technique and obtained from the *stratum lacunosum-moleculare* for illustrative purposes. **A,B,D,E,G,H**. In all those animals and ages, $GABA_{B1}$ immunoparticles were found along the extrasynaptic plasma membrane (arrows) and intracellular sites (crossed arrows) of dendritic shafts (Den) and spines (s) of CA1 pyramidal cells contacted by axon terminals (at), and less frequently at presynaptic sites (arrowheads). **C**. Quantitative analysis at 1 month in the *strata radiatum* and *lacunosum-moleculare* showed that the proportion of postsynaptic $GABA_{B1}$ immunoparticles along the plasma membrane (65.52% in *sr* and 65.11% in *slm*) and intracellular sites (34.48% in *sr* and 34.89% in *slm*) in APP/PS1 was similar to age-matched wild-type mice (Plasma membrane: 64.04% in *sr* and 64.68% in *slm*; Intracellular: 35.96% in *sr* and 35.32% in *slm*) in dendritic spines and shafts of CA1 pyramidal cells. **F**. Quantitative analysis at 6 months showed no changes in the *stratum radiatum* (Plasma membrane: 63.45% in wild type and 63.46% in APP/PS1; Intracellular: 36.55% in wild type and 36.54% in APP/PS1), but a clear reduction of plasma membrane $GABA_{B1}$ at postsynaptic compartments, with a subsequent increase in cytoplasmic sites, in APP/PS1 mice (Plasma membrane: 62.06% in wild type and 41.05% in APP/PS1; Intracellular: 37.94% in wild type and 58.05% in APP/PS1). (I) Quantitative analysis at 12 months of age showing that $GABA_{B1}$ immunoparticles were less frequently observed along the extrasynaptic plasma membrane dendrites and spines of CA1 pyramidal cells in APP/PS1 mice, as well at presynaptic sites, but instead they more frequently detected at intracellular sites in both the *strata radiatum* (Plasma membrane: 58.81% in wild type and 32.60% in APP/PS1; Intracellular: 41.19% in wild type and 67.40% in APP/PS1), proximal and distal parts, and *lacunosum-moleculare* (Plasma membrane: 54.23% in wild type and 15.19% in APP/PS1; Intracellular: 45.77% in wild type and 84.81% in APP/PS1). Scale bars: A,B,D,E, 1 μm; G,H, 0.5 μm.

Intracellular: 39.22% in wild type and 66.67% in APP/PS1) and *stratum lacunosum-moleculare* (Plasma membrane: 65.22% in wild type and 31.25% in APP/PS1; Intracellular: 34.78% in wild type and 68.75% in APP/PS1) (Figure 9I).

Finally, to validate the described reduction of post and presynaptic $GABA_B$ receptors in the hippocampus of APP/PS1 mice, we determined their expression levels together with other markers in human tissue. Thus, using

immunoblots we assessed the expression levels of $GABA_{B1}$, GluA1, GluA2 and GluN1 in tissue lysates of the hippocampus in control and AD cases (Supplementary Figure S3A). Quantification of all these immunoreactive bands revealed that $GABA_{B1}$, GluA1, GluA2 and GluN1 proteins were significantly reduced in the hippocampus of AD subjects compared to controls (Supplementary Figure S3B).

DISCUSSION

To understand the mechanisms that are operative in AD, it is important to appreciate that alteration of neurotransmitter receptors must be a common denominator of dendritic spines loss and synaptic impairment, two critical events in the pathophysiology of this neurodegenerative disease (42, 48, 54). We hypothesize that neurons experiencing AD neuropathology may selectively regulate neurotransmitter receptors associated with excitatory synapses, thus contributing to neuronal damage and to the cognitive decline associated with AD. However, the receptors and ion channels involved in the synaptic deficits present in pathological conditions are still poorly known. Identification of the molecular mechanisms at central synapses affected by AD may allow developing more effective therapeutic approaches for AD, for which no curative treatment is yet available. Here, we have demonstrated for the first time a compartment- and age-dependent reduction of surface $GABA_B$ receptors and a parallel intracellular increase of these receptors in CA1 pyramidal cells with progressive neuropathology in an AD mouse model, the APP/PS1 model. We additionally show that the decrease of $GABA_B$ receptors also affects in an age-dependent manner axon terminals contacting CA1 pyramidal cells. The significant reduction in $GABA_B$ receptors may contribute to the pathology and memory impairment associated with AD.

Unchanged expression of hippocampal $GABA_B$ receptor protein in Alzheimer's disease

Dysfunction of the hippocampus largely contributes to the memory deficits that characterise AD (31, 44). In contrast to the large interest focused on the potential role of glutamate receptors in AD (11, 39), less information is available about the involvement of GABA receptors. In particular, $GABA_B$ receptors also play a role in learning and memory (19). Recent studies reported that $GABA_B$ receptors selectively co-purify with APP (47) and this macromolecular complex links presynaptic $GABA_B$ receptor trafficking to Aβ formation (9). In addition, $GABA_{B1a}$ has been identified as a receptor for secreted APP, which would regulate the function of the receptor isoform to modulate synaptic transmission and plasticity (45). For these reasons, our work adopted transgenic mice overexpressing mutant familial AD genes [amyloid-β protein precursor (AβPP), presenilin-1 (PS1), and PS2], considered one of the most relevant animal models of AD. These animals show Aβ deposition by 4 months with a progressive increase in senile plaque number up to 12 months and cognitive impairments (14, 15).

In the present study, we demonstrated with different approaches that total protein levels of $GABA_B$ receptors were not significantly changed in APP/PS1 mice with the progressive increase of Aβ levels at different ages in the hippocampus. This does not seems to be the case for other components of the GABA receptor systems, as $GABA_A$ receptors are differentially affected in AD in a region- and subunit-dependent manner. Thus, some $GABA_A$ subunits showed decrease expression in the human hippocampus, although some others remain unchanged (28). In contrast, our data also show reduction of $GABA_{B1}$ protein level in the hippocampus of AD patients, consistent with the reported downregulation in the gene expression of $GABA_{B1}$ in AD (43). This discrepancy could be due to posttranscriptional changes in the control of gene expression at the RNA level, but more likely could be the result of differences in brain organisation between humans and mice, because the APP/PS1 model does not develop neurofibrillary tangles, other typical pathologic alterations observed in AD human patients, or because the stages of AD in the patients were more severe than the AD neuropathology suffered by mice at 12 months of age.

Ultrastructural studies in the hippocampus have shown that $GABA_B$ receptors are enriched in the vicinity of excitatory synapses, supporting the idea that glutamate receptors can influence $GABA_B$ receptor signaling (27, 32, 53). Indeed, NMDA receptor activation can induce phosphorylation on the $GABA_{B1}$ and $GABA_{B2}$ subunits to promote endocytosis (17, 51). $GABA_B$ receptors can also influence the NMDA-mediated excitatory postsynaptic potentials in the CA1 region of the hippocampus (38). An autoradiography study of $GABA_B$ receptor expression in the human hippocampus of AD patients indicated fewer $GABA_B$ receptors in the molecular layer of the dentate gyrus, and the *strata pyramidale* and *lacunosum-moleculare* of the CA1 region (7). Our current knowledge of the complexity of receptor organization in central neurons demands more exacting techniques that allow precise identification and localization of individual receptor subtypes to unravel their distribution in AD. Thus, the SDS-FRL and pre-embedding immunogold techniques were the methods of choice to decipher the density of $GABA_{B1}$ in hippocampal neurons.

Plasma membrane reduction of $GABA_B$ receptors in the hippocampus of Alzheimer's disease

One of the major research aims in this work has been to examine the possibility that, despite the unchanged protein levels in the APP/PS1 model of AD, $GABA_B$ receptors may still undergo changes in their localization along the plasma membrane vs. cytoplasmic sites with pathology progression. For that purpose we concentrated in the CA1 region of the hippocampus using the SDS-FRL technology, proved to be an excellent tool to study the high-resolution subcellular localization of surface-localized proteins (50). Using this technique, we were able

to fully map the two-dimensional distribution of $GABA_B$ receptors obtaining very accurate data about their density in different compartments of CA1 pyramidal cells in brains displaying AD pathology at a level of detail never previously attained.

Our analysis revealing that $GABA_B$ receptors are differentially localized to somato-dendritic compartments of hippocampal principal cells, both in wild type and APP/PS1 at the three ages studied is in line with results of previous immunoEM investigations performed in young adult animals (12, 27, 32, 53). More importantly, the principal and exciting finding from our results is the reduction in the density of plasma membrane-targeted $GABA_B$ receptors in an age- and compartment-dependent manner. Thus, we detected significant differences in the plasma membrane distribution of $GABA_{B1}$ and subsequent increase at cytoplasmic sites only in the *stratum lacunosum-moleculare*, but found no evidence for changes in all other pyramidal cell compartments, at 6 months of age. This observation is consistent with the evidence that density of binding sites for $GABA_B$ receptors are decreased in *stratum lacunosum-moleculare* of the CA1 region in human hippocampus with AD (7). Since this hippocampal region is the common location for large accumulation of Aβ in AD (22), the decrease in density of surface $GABA_{B1}$ in the *stratum lacunosum-moleculare* of the CA1 region may reflect changes due to entorhinal cortical pathology. Previous work demonstrated that AD pathology begins in the entorhinal cortex and spreads through synaptic connections to the hippocampus (31) and the resulting hippocampal synaptic weakening induced in the entorhinal cortex is a consequence of the pathologic increase of Aβ and p-tau (49).

At more advanced stages of AD pathology APP/PS1 mice show high-density of Aβ and severe cognitive impairments develop (2, 15). Our analysis performed at 12 months of age revealed a significant reduction in the membrane surface distribution of $GABA_{B1}$ in all neuronal compartments. The possibility that these immunohistochemical findings in APP/PS1 are due to technical issues or storage conditions is unlikely because wild-type and APP/PS1 mice were always matched from same litters and although dystrophic dendrites were observed in these transgenic mice (2) our investigation was performed in the Aβ plaque-free regions from these animals. Following the finding on the reduction of $GABA_{B1}$ along the membrane surface of CA1 pyramidal cells in APP/PS1 mice, we investigated potential internalization at cytoplasmic sites. Immunoelectron microscopy and quantitative analysis showed that there is an accumulation of immunoparticles for $GABA_{B1}$ at cytoplasmic sites. Given that the total amount of $GABA_{B1}$ protein does not change between wild-type and APP/PS1 mice, our data suggests that the internalized pool of $GABA_B$ receptors was not redirected to subsequent lysosomal degradation in AD, in contrast to the activity-dependent degradation of $GABA_B$ receptors observed in hippocampal and cortical neurons (17, 51). Similar plasma membrane-cytoplasmic redistribution of $GABA_B$ receptors has been reported in GABAergic neurons of the VTA in methamphetamine-injected mice (39).

An additional, interesting finding of the present study is that reduction of membrane surface $GABA_{B1}$ in our model of AD was due to alteration in its clustering, with lower number of clusters and fewer immunoparticles per cluster. $GABA_B$ receptors form macromolecular signaling complexes with GIRK channels and Cav channels (40). Although no information is yet available about the alterations of these effector ion channels in AD, the decrease of $GABA_B$ receptors from the membrane surface of CA1 pyramidal cells, together with the decrease of GIRK2 channels we detected in the same compartments, can produce alteration in $GABA_B$-mediated GIRK currents (39) and this could involve a change in G protein-coupling efficiency with effector ion channels (29) or simply that fewer receptors can couple to channels. Altogether, this alteration might be enough to reduce GIRK and/or Cav channel conductance in CA1 pyramidal neurons, thus playing a potential role in the hippocampal activity dysfunction observed in AD, although this needs to be confirmed with electrophysiology.

On the presynaptic side, $GABA_B$ receptors mediate slow and prolonged synaptic inhibition by activating Cav channels, thus modulating the release of neurotransmitters (3). In the hippocampus, synaptically released GABA can inhibit excitatory neurotransmission at the Schaffer collateral synapses in CA1 acting through presynaptic $GABA_B$ receptors (24). In this study we observed immunoparticles for $GABA_{B1}$ along the extrasynaptic membrane and the active zone or presynaptic membrane specialization of axon terminals in different layers of the CA1 region, in line with previous reports using different ultrastructural approaches (27, 53). Similarly to the decrease of postsynaptic $GABA_B$ receptors, we detected a reduction of presynaptic $GABA_{B1}$ in APP/PS1 mice of 12 months and this reduction was more pronounced in the *stratum lacunosum-moleculare*. This data are in agreement with a recent study reporting that the increase in Aβ production is linked to dysfunctional axonal trafficking and reduced $GABA_B$ receptor expression in the APP-/- mice (9) and also consistent with the study showing that secreted APP binds to $GABA_{B1a}$ (45), an isoform preferentially localized at presynaptic sites (53), to supress synaptic vesicle release and thus modulating synaptic transmission and plasticity. One way to reduce or supress the release of neurotransmitter from synaptic vesicles is by decreasing the number of involved receptors in the presynaptic plasma membrane, consistent with the reduction of $GABA_B$ receptors we have reported at presynaptic sites.

CONCLUSIONS

Our work explored the pre and postsynaptic alteration of $GABA_B$ receptors in hippocampal CA1 pyramidal cells in a mouse model of AD, providing new insights into neurotransmitter receptor redistribution at different stages of AD pathology. This work shows a severe reduction of membrane surface $GABA_B$ receptors and subsequent accumulation at

cytoplasmic sites only at those ages and in those neuronal compartments suffering a decrease from the plasma membrane. The mechanisms behind these changes in subcellular distribution and their functional implications are still not known. However, the present study and future data in human tissue are important to explore how $GABA_B$ receptors are involved in the altered neuronal excitability associated with AD, essential information for the development of therapeutic strategies for disease improvement. One way of therapeutic intervention would be stabilizing of $GABA_B$ receptors in the neuronal surface, controlled by heteromerization with other proteins, and by phosphorylation and dephosphorylation events, and regulated by changes in glutamatergic excitatory activity.

ACKNOWLEDGMENTS

The authors are grateful to Prof. Elek Molnar for providing the rabbit pan-AMPA antibody. Funding sources were European Union's Horizon 2020 Framework Programme for Research and Innovation, Spanish Ministerio de Economía y Competitividad, Junta de Comunidades de Castilla-La Mancha (Spain) and Life Science Innovation Center at University of Fukui.

This project/research has received funding from the European Union's Horizon 2020 Framework Programme for Research and Innovation under the Specific Grant Agreement No. 785907 (Human Brain Project SGA2) to RL. This work was supported by grants from the Spanish Ministerio de Economía y Competitividad (BFU2015-63769-R and RTI2018-095812-B-I00) and Junta de Comunidades de Castilla-La Mancha (SBPLY/17/180501/000229) to RL, and Life Science Innovation Center (Research and Education Program for Life Science) at University of Fukui and JSPS KAKENHI Grant Numbers 16H04662, 17K19446 and 18H05120 to YF.

CONFLICT OF INTEREST

The authors of this manuscript declare that they have no conflict of interests.

AUTHOR CONTRIBUTIONS

All authors had full access to all data in the study and take responsibility for the integrity of the data and the accuracy of the data analysis. RL and YF designed the project; AMB, RL and YF performed SDS- FRL immunoelectron microscopy; AMB, CA and AEMM performed histoblot analysis; AMB performed western blots; AMB, RAR and AEMM performed light microscopy immunohistochemistry; LDLO developed in-house software and performed computational analysis; RS provided reagents and feedback on the quantitative analysis; JMH and AB provided APP/PS1 and WT tissues and feedback on the manuscript; SF and BB provided knock-out tissues and feedback on the manuscript; AMB, RAR, CA and RL analysed data; RL wrote the paper. All authors read and approved the final manuscript.

CONSENT FOR PUBLICATION

All co-authors of the present manuscript can certify that it has not been submitted to more than one journal for simultaneous consideration and that the manuscript has not been published previously (partly or in full). The authors also can certify that our main study is not split up into several parts to increase the quantity of submissions, that none of the data presented here have been fabricated or manipulated and that we present our own data/text/theories/ideas. All authors and authorities have explicitly provided their consent to submit the present manuscript and in general we all agree with the ethical responsibilities of authors of the journal. Finally, all authors give consent for publication in *Brain Pathology*.

DATA AVAILABILITY STATEMENT

All data used and/or analyzed during the current study were available from the corresponding author on reasonable request.

ETHICAL APPROVAL AND CONSENT TO PARTICIPATE

All animal experimental procedures were performed in accordance with Spanish (RD 1201/2015) and European Union regulations (86/609/EC) and the protocols were approved by the local Animal Care and Use Committee.

REFERENCES

1. Aguado C, Luján R. (2019) The histoblot technique: a reliable approach to analyse expression profile of proteins and to predict their molecular association. In: Co-immunoprecipitation Methods for Brain Tissue, Neuromethods, vol. **144**, Y Odagaki, DO Borroto-Escuela (eds), pp. 65–88. Humana Press: New York, NY.
2. Alonso-Nanclares L, Merino-Serrais P, Gonzalez S, DeFelipe J (2013) Synaptic changes in the dentate gyrus of APP/PS1 transgenic mice revealed by electron microscopy. *J Neuropathol Exp Neurol* **72**:386–395.
3. Bettler B, Kaupmann K, Mosbacher J, Gassmann M (2004) Molecular structure and physiological functions of GABA(B) receptors. *Physiol Rev* **84**:835–67.
4. Bischoff S, Leonhard S, Reymann N, Schuler V, Shigemoto R, Kaupmann K, Bettler B (1999) Spatial distribution of GABABR1 receptor mRNA and binding sites in the rat brain. *J Comp Neurol* **412**:1–16.
5. Bloom GS (2014) Amyloid-β and tau: the trigger and bullet in Alzheimer disease pathogenesis. *JAMA Neurol* **71**:505–508.
6. Chu DCM, Albin RL, Young AB, Penney JB (1990) Distribution and kinetics of $GABA_B$ binding sites in rat central nervous system: a quantitative autoradiographic study. *Neuroscience* **34**:341–357.
7. Chu DCM, Penny JB, Young AB (1987) Cortical GABAB and GABAA receptors in Alzheimer's disease: a quantitative autoradiographic study. *Neurology* **37**:1454–1459.

8. Degro CE, Kulik A, Booker SA, Vida I (2015) Compartmental distribution of GABAB receptor-mediated currents along the somatodendritic axis of hippocampal principal cells. *Front Synaptic Neurosci* **7**:6.
9. Dinamarca MC, Raveh A, Schneider A, Fritzius T, Früh S, Rem PD *et al* (2019) Complex formation of APP with $GABA_B$ receptors links axonal trafficking to amyloidogenic processing. *Nat Commun* **10**:1331.
10. Fernández-Alacid L, Watanabe M, Molnár E, Wickman K, Luján R (2011) Developmental regulation of G protein-gated inwardly-rectifying K+ (GIRK/Kir3) channel subunits in the brain. *Eur J Neurosci* **34**:1724–1736.
11. Forner S, Baglietto-Vargas D, Martini AC, Trujillo-Estrada L, LaFeria FM (2017) Synaptic impairment in Alzheimer's disease: A dysregulated symphony. *Trends Neurosci* **40**:347–357.
12. Fritschy JM, Meseknaite V, Weinmann O, Honer M, Benke D, Mohler H (1999) $GABA_B$-receptor splice variants GB1a and GB1b in rat brain: developmental regulation, cellular distribution and extrasynaptic localization. *Eur J Neurosci* **11**:761–768.
13. Fritschy JM, Panzanelli P (2014) GABAA receptors and plasticity of inhibitory neurotransmission in the central nervous system. *Eur J Neurosci* **39**:1845–1865.
14. Garcia-Alloza M, Robbins EM, Zhang-Nunes SX, Purcell SM, Betensky RA, Raju S *et al* (2006) Characterization of amyloid deposition in the APPswe/PS1dE9 mouse model of Alzheimer disease. *Neurobiol Dis* **24**:516–524.
15. Gimbel DA, Nygaard HB, Coffey EE, Gunther EC, Laurén J, Gimbel ZA, Strittmatter SM (2010) Memory impairment in transgenic Alzheimer mice requires cellular prion protein. *J Neurosci* **30**:6367–6374.
16. Gray EG (1959) Electron microscopy of synaptic contacts on dendrite spines of the cerebral cortex. *Nature* **183**:1592–1593.
17. Guetg N, Abdel Aziz S, Holbro N, Turecek R, Rose T, Seddik R *et al* (2010) NMDA receptor-dependent GABAB receptor internalization via CaMKII phosphorylation of serine 867 in GABAB1. *Proc Natl Acad Sci U S A* **107**:13924–13929.
18. Haller C, Casanova E, Müller M, Vacher CM, Vigot R, Doll T *et al* (2004) Floxed allele for conditional inactivation of the GABAB(1) gene. *Genesis* **40**:125–130.
19. Helm KA, Haberman RP, Dean SL, Hoyt EC, Melcher T, Lund PK, Gallagher M (2005) GABAB receptor antagonist SGS742 improves spatial memory and reduces protein binding to the cAMP response element (CRE) in the hippocampus. *Neuropharmacology* **48**:956–964.
20. Hsieh H, Boehm J, Sato C, Iwatsubo T, Tomita T, Sisodia S, Malinow R (2006) AMPAR removal underlies Abeta-induced synaptic depression and dendritic spine loss. *Neuron* **52**:831–843.
21. Huang Y, Mucke L (2012) Alzheimer mechanisms and therapeutic strategies. *Cell* **148**:1204–1222.
22. Hyman BT, Van Hoesen GW, Damasio AR, Barnes CL (1984) Alzheimer's disease: cell-specific pathology isolates the hippocampal formation. *Science* **225**:1168–1170.
23. Indriati DW, Kamasawa N, Matsui K, Meredith AL, Watanabe M, Shigemoto R (2013) Quantitative localization of Cav2.1 (P/Q-type) voltage-dependent calcium channels in Purkinje cells: somatodendritic gradient and distinct somatic coclustering with calcium-activated potassium channels. *J Neurosci* **33**:3668–3678.
24. Isaacson JS, Solís JM, Nicoll RA (1993) Local and diffuse synaptic actions of GABA in the hippocampus. *Neuron* **10**:165–175.
25. Kaupmann K, Huggel K, Heid J, Flor PJ, Bischoff S, Mickel SJ *et al* (1997) Expression cloning of $GABA_B$ receptors uncovers similarity to metabotropic glutamate receptors. *Nature* **386**:239–246.
26. Kulik A, Nakadate K, Nyíri G, Notomi T, Malitschek B, Bettler B, Shigemoto R (2002) Distinct localization of GABA(B) receptors relative to synaptic sites in the rat cerebellum and ventrobasal thalamus. *Eur J Neurosci* **15**:291–307.
27. Kulik A, Vida I, Luján R, Haas CA, López-Bendito G, Shigemoto R, Frotscher M (2003) Subcellular localization of metabotropic GABA(B) receptor subunits GABA(B1a/b) and GABA(B2) in the rat hippocampus. *J Neurosci* **23**:11026–11035.
28. Kwakowsky A, Calvo-Flores Guzmán B, Pandya M, Turner C, Waldvogel HJ, Faull RL (2018) $GABA_A$ receptor subunit expression changes in the human Alzheimer's disease hippocampus, subiculum, entorhinal cortex and superior temporal gyrus. *J Neurochem* **145**:374–392.
29. Labouèbe G, Lomazzi M, Cruz HG, Creton C, Luján R, Li M *et al* (2007) RGS2 modulates coupling between GABAB receptors and GIRK channels in dopamine neurons of the ventral tegmental area. *Nat Neurosci* **10**:1559–1568.
30. Lamprecht R, LeDoux J (2004) Structural plasticity and memory. *Nat Rev Neurosci* **5**:45–54.
31. Llorens-Martín M, Blazquez-Llorca L, Benavides-Piccione R, Rabano A, Hernández F, Ávila J, DeFelipe J (2014) Selective alterations of neurons and circuits related to early memory loss in Alzheimer's disease. *Front Neuroanat* **8**:38.
32. López-Bendito G, Shigemoto R, Kulik A, Vida I, Fairén A, Luján R (2004) Distribution of metabotropic GABA receptor subunits GABAB1a/b and GABAB2 in the rat hippocampus during prenatal and postnatal development. *Hippocampus* **14**:836–848.
33. Luján R, Aguado C, Ciruela F, Cózar J, Kleindienst D, de la Ossa L *et al* (2018) Differential association of $GABA_B$ receptors with their effector ion channels in Purkinje cells. *Brain Struct Funct* **223**:1565–1587.
34. Luján R, Nusser Z, Roberts JD, Shigemoto R, Somogyi P (1996) Perisynaptic location of metabotropic glutamate receptors mGluR1 and mGluR5 on dendrites and dendritic spines in the rat hippocampus. *Eur J Neurosci* **8**:1488–1500.
35. Luján R, Shigemoto R (2006) Localization of metabotropic GABA receptor subunits GABAB1 and GABAB2 relative to synaptic sites in the rat developing cerebellum. *Eur J Neurosci* **23**:1479–1490.
36. Malinow R (2012) New developments on the role of NMDA receptors in Alzheimer's disease. *Curr Opin Neurobiol* **22**:559–563.
37. Marshall FH, Jones KA, Kaupmann K, Bettler B (1999) Gaba-B receptors: the first 7TM heterodimers. *Trends Pharmacol Sci* **20**:396–399.
38. Morrisett RA, Mott DD, Lewis DV, Swartzwelder HS, Wilson WA (1991) GABAB-receptor-mediated inhibition of the N-methyl-D-aspartate component of synaptic transmission in the rat hippocampus. *J Neurosci* **11**:203–209.
39. Padgett CL, Lalive AL, Tan KR, Terunuma M, Munoz MB, Pangalos MN *et al* (2012) Methamphetamine-evoked depression of GABA(B) receptor signaling in GABA neurons of the VTA. *Neuron* **73**:978–989.
40. Padgett CL, Slesinger PA (2010) GABAB receptor coupling to G-proteins and ion channels. *Adv Pharmacol* **58**:123–47.

41. Paula-Lima AC, Brito-Moreira J, Ferreira ST (2013) Deregulation of excitatory neurotransmission underlying synapse failure in Alzheimer's disease. *J Neurochem* **126**:191–202.
42. Penzes P, Cahill ME, Jones KA, VanLeeuwen JE, Woolfrey KM (2011) Dendritic spine pathology in neuropsychiatric disorders. *Nat Neurosci* **14**:285–293.
43. Puthiyedth N, Riveros C, Berretta R, Moscato P (2016) Identification of differentially expressed genes through integrated study of Alzheimer's Disease affected brain regions. *PLoS ONE* **11**:e0152342.
44. Revett TJ, Baker GB, Jhamandas J, Kar S (2013) Glutamate system, amyloid ß peptides and tau protein: functional interrelationships and relevance to Alzheimer disease pathology. *J Psychiatry Neurosci* **38**:6–23.
45. Rice HC, de Malmazet D, Schreurs A, Frere S, Van Molle I, Volkov AN *et al* (2019) Secreted amyloid-β precursor protein functions as a $GABA_B$R1a ligand to modulate synaptic transmission. *Science* **363**:eaao4827.
46. Scheuner D, Eckman C, Jensen M, Song X, Citron M, Suzuki N *et al* (1996) Secreted amyloid beta-protein similar to that in the senile plaques of Alzheimer's disease is increased in vivo by the presenilin 1 and 2 and APP mutations linked to familial Alzheimer's disease. *Nat Med* **2**:864–870.
47. Schwenk J, Pérez-Garci E, Schneider A, Kollewe A, Gauthier-Kemper A, Fritzius T *et al* (2016) Modular composition and dynamics of native GABAB receptors identified by high-resolution proteomics. *Nat Neurosci* **19**:233–242.
48. Selkoe DJ (2002) Alzheimer's disease is a synaptic failure. *Science* **298**:789–791.
49. Spires-Jones TL, Hyman BT (2014) The intersection of amyloid beta and tau at synapses in Alzheimer's disease. *Neuron* **82**:756–771.
50. Tanaka J, Matsuzaki M, Tarusawa E, Momiyama A, Molnar E, Kasai H, Shigemoto R (2005) Number and density of AMPA receptors in single synapses in immature cerebellum. *J Neurosci* **25**:799–807.
51. Terunuma M, Vargas KJ, Wilkins ME, Ramírez OA, Jaureguiberry-Bravo M, Pangalos MN *et al* (2010) Prolonged activation of NMDA receptors promotes dephosphorylation and alters postendocytic sorting of GABAB receptors. *Proc Natl Acad Sci U S A* **107**:13918–13923.
52. Tönnes J, Stierli B, Cerletti C, Behrmann JT, Molnar E, Streit P (1999) Regional distribution and developmental changes of GluR1-flop protein revealed by monoclonal antibody in rat brain. *J Neurochem* **73**:2195–2205.
53. Vigot R, Barbieri S, Bräuner-Osborne H, Turecek R, Shigemoto R, Zhang YP *et al* (2006) Differential compartmentalization and distinct functions of GABAB receptor variants. *Neuron* **50**:589–601.
54. Walsh DM, Selkoe DJ (2004) Deciphering the molecular basis of memory failure in Alzheimer's disease. *Neuron* **44**:181–193.
55. Wang R, Reddy PH (2017) Role of Glutamate and NMDA Receptors in Alzheimer's Disease. *J Alzheimers Dis* **57**:1041–1048.
56. West MJ, Kawas CH, Martin LJ, Troncoso JC (2000) The CA1 region of the human hippocampus is a hot spot in Alzheimer's disease. *Ann N Y Acad Sci* **908**:255–259.
57. West MJ, Kawas CH, Stewart WF, Rudow GL, Troncoso JC (2004) Hippocampal neurons in pre-clinical Alzheimer's disease. *Neurobiol Aging* **25**:1205–1212.
58. Whitehead G, Regan P, Whitcomb DJ, Cho K (2017) Ca_{2+}-permeable AMPA receptor: A new perspective on amyloid-beta mediated pathophysiology of Alzheimer's disease. *Neuropharmacology* **112**:221–227.
59. Zhang Y, Li P, Feng J, Wu M (2016) Dysfunction of NMDA receptors in Alzheimer's disease. *Neurol Sci* **37**:1039–1047.

SUPPORTING INFORMATION

Additional supporting information may be found in the online version of this article at the publisher's web site:

Figure S1. *Reduced density of synaptic AMPA receptors in dendritic spines of APP/PS1 mice at 12 months*. (**A-F**) Electron micrographs of the hippocampus showing immunoparticles for pan-AMPA at excitatory synaptic sites of dendritic spines of pyramidal cells in the CA1 *stratum lacunosum-moleculare*, as detected using the SDS-FRL technique at 1, 6 and 12 months of age. Postsynaptic membrane specializations (IMP clusters, pseudo coloured in blue for wild type and in red for APP/PS1 to aid visualization) show strong immunoreactivity for pan-AMPA (10 nm gold particles) in the wild type, while they show weaker immunoreactivity in the APP/PS1. Scale bars: **A-F**, 200 nm. (**G,H,I**) Histograms showing the distribution of densities of gold particles that label AMPA receptors in SDS-FRL replicas of individual postsynaptic membrane specializations in wild type and APP/PS1 mice. Quantitative analysis showed no changes in the densities of AMPA immunoparticles in excitatory synapses in dendritic spines at 1 and 6 months of age (panels **G** and **H**). However, the analysis showed a significant reduction in the APP/PS1 mice (205.03 ± 16.88 immunoparticles/μm^2) compared to age matched wild type (423.20 ± 20.33 immunoparticles/μm^2; Kruskal–Wallis test, pairwise Mann–Whitney U test and Dunn's method, $***P < 0.001$) at 12 months of age. Error bars indicate SEM.

Figure S2. *Reduced density of synaptic markers in APP/PS1 mice at 12 months*. (**A-F**) Electron micrographs of the hippocampus showing immunoparticles for the GluN1 subunit of the NMDA receptors, the GIRK2 subunit of GIRK channels and SNP-25 in the CA1 *stratum lacunosum-moleculare*, as detected using the SDS-FRL technique at 12 months of age. (**A,D**) Strong immunoreactivity for GluN1 (10 nm gold particles) were observed in postsynaptic membrane specializations in the wild type, while weaker immunoreactivity was detected in the APP/PS1. (**G**) Quantitative analysis showing a significant reduction of in the APP/PS1 mice (68.74 ± 11.15 immunoparticles/μm2) compared to age matched wild type (198.56 ± 15.24 immunoparticles/μm2; Kruskal–Wallis test, pairwise Mann–Whitney U test and Dunn's method, ***p<0.0001). (**B,E**) Immunoparticles for GIRK2 were observed along the surface membrane of dendrites and spines. (**H**) Quantitative analysis showing that immunoreactivity for GIRK2 was significantly reduced in oblique dendrites (oDen) and spines in APP/PS1 mice (oDen = 92.74 ± 18.12 immunoparticles/μm^2, n = 10 dendrites; s = 128.00 ± 12.38 immunoparticles/μm^2, n = 9 spines) compared to age-match wild type mice oDen = 273.10 ± 25.92 immunoparticles/μm^2, n = 10

dendrites; s = 461.92 ± 59.88 immunoparticles/μm^2, n = 10 spines) (Two-way ANOVA test, $*P < 0.05$; $***P < 0.01$). (**C,F**) Immunoreactivity for SNAP-25 were detected along the extrasynaptic plasma membrane of axon terminals (at) facing dendritic spines (s). (**I**) Our quantitative analysis showed a significant reduction in the density of SNAP-25 in the APP/PS1 mice (30.73 ± 7.58 immunoparticles/μm^2) compared to age matched wild type (mean = 134.02 ± 7.46 immunoparticles/μm^2; t test using Holm-Sidak method, $***P < 0.001$). Scale bars: **A-F**, 200 nm. Error bars indicate SEM.

Figure S3. *Co-localization of $GABA_B$ receptors with marker proteins in APP/PS1 mice at 12 months*. (**A-H**) Immunofluorescence for $GABA_{B1}$ (green) and Rab4 (red), EEA1 (red), LAMP1 (red) or CHOP (red) in wild type and APP/PS1 mice at 12 months of age. The overlay between $GABA_{B1}$ and each marker protein can be seen in yellow (A3-G3, B3-H3). Co-localization between $GABA_{B1}$ and the different marker proteins was detected mainly in the somata of pyramidal cells in the *stratum pyramidale*, but no differences in the frequency of co-localization was observed in the APP/PS1 mice compared to age-matched controls. so, *stratum oriens*; sr, *stratum radiatum*. Scale bars: **A-H**, 20 μm.

Figure S4. *Representative western blots of different molecules in the hippocampus from control and Alzheimer´s patients*. (**A**) Crude membrane preparations were subjected to 7.5% SDS-PAGE, transferred on to polyvinylidene difluoride membranes. They were reacted with an anti-pan $GABA_{B1}$ antibody, which recognised both $GABA_{B1a}$ and $GABA_{B1b}$ subunits with estimated molecular masses of 130 and 100 kDa, respectively. The antibodies to GluA1, GluA2 detected a single predominant band at 100 kDa and NMDA detected a single predominant band at 120 kDs. (**B**) The developed immunoblots were scanned and densitometric measurements were averaged together to compare the protein densities between controls and AD in the hippocampus. Quantification of $GABA_{B1}$, GluA1, GluA2 and GluN1 normalised to α-tubulin and expressed as pixel density showed a significant reduction in the amount of proteins when compared AD with controls. An antibody anti α-Tubulin served as an internal control to ensure comparable protein loading showed no significant difference among AD or control groups. Data are means ± SEM of represented cases. $*P < 0.05$; $**P < 0.01$; $***P < 0.001$.

Figure S5. *The density of CA1 pyramidal cells is not altered in APP/PS1 mice at 12 months*. (**A**) Hippocampal sections from WT and APP/PS1 were stained with DAPI. (**B**) Quantification of the number of nuclei in the pyramidal cell layer of the CA1 region. We confirmed that the number of neurons is similar between WT and APP/PS1. Scale bars: **A-B**, 100 μm.